Option Pricing with Dynamic Conditional Skewness

January 30, 2024

Abstract

In this paper, we develop a discrete-time affine option-pricing model that explicitly incorporates the dynamics of conditional skewness. The new proposed model features different dynamics for conditional skewness and variance. To stress the difference in information, we use alternative realized measures constructed from high-frequency historical returns to update skewness and variance dynamics. By Fourier inversion, we derive closed-form option valuation formulas. Empirically, the flexibility that the model offers for conditional skewness as well as high-frequency information from the underlying asset contribute to superior performance upon benchmark models using S&P 500 index options. Overall, the joint modeling of dynamic conditional skewness and realized measures leads to an out-of-sample gain of 12.25% in pricing accuracy. The improvements are more pronounced for deep in-the-money calls, options with shorter maturities, and during highly volatile periods.

Keywords: Dynamic Conditional Skewness, Realized Skewness, Inverse Gaussian Distribution, Option Pricing

JEL Classification: G13, C58, C51

1 Introduction

Deviations between option market prices and theoretical prices from the Black–Scholes formula have been extensively documented in the existing literature. Specifically, out-of-the-money (OTM) put prices are higher than corresponding Black–Scholes prices. The empirical fact is also known as the "volatility smirk". To capture the deviations and thus improve option pricing accuracy, an early method is to model conditional heteroskedasticity (see, for example, Heston (1993), Ding and Granger (1996), and Jones (2003)). On this basis, the pricing accuracy of option valuation models with conditional heteroskedasticity can be further improved by incorporating leverage parameters (see Heston and Nandi (2000), Christoffersen and Jacobs (2004), Christoffersen et al. (2014), and Feunou and Okou (2019), among others).

Leverage parameters in models with conditional heteroskedasticity measure the leverage effect, that is, a negative shock in return increases the volatility more than a positive shock of equal magnitude. This increases the probability of a large drop in the return of the underlying asset and thus the value of the OTM put options. This implication of the leverage effect is equivalent to negative skewness in returns (Christoffersen et al. (2006)). In addition to the leverage effect on the multi-period correlation between return and volatility, single-period return is also skewed (Neuberger (2012)). While the leverage effect generates negative skewness in multi-period returns, innovations in single-period return equations are still assumed to be Gaussian distributed in these models. Therefore, modeling conditional heteroskedasticity and incorporating leverage parameters are not sufficient to explain observed deviations from Black-Scholes (BS, Black and Scholes (1973)) prices for options with short maturities.

To explain price deviations for options with short maturities, Christoffersen et al. (2006) model the innovation in return equation using an inverse Gaussian distribution with nonzero third moment to generate negative skewness in single-period returns, and refer to this model as the inverse Gaussian GARCH model. However, the dynamics of the conditional skewness in the inverse Gaussian GARCH model are completely determined by the dynamics of the conditional variance. Furthermore, only daily returns are used to update the dynamics of the conditional variance and thus the skewness.

To compare the dynamics of skewness and volatility of underlying asset returns, Figure 1 plots the time series of the Cboe SKEW Index (SKEW) and the Cboe Volatility Index (VIX). VIX is a

measure of 30-day expected volatility of the S&P 500 Index (SPX), derived from prices of SPX call and put options. Similar to VIX, SKEW estimates the skewness of S&P 500 returns at the end of a 30-day horizon, calculated from the prices of S&P 500 out-of-the-money options.[1] We observe that SKEW exhibits dynamic behavior rather than fluctuating around a specific level, indicating continuous market adjustments in skewness expectations. Moreover, the increasing variation of SKEW in recent years underscores the growing importance of accurately modeling skewness and the heightened market attention to skewness risks. Importantly, the dynamic patterns and evolution tracks of SKEW are related to, but not completely determined by, VIX, providing direct evidence for additional information content and different specifications to determine the dynamics of skewness and volatility.

[1] VIX methodology: https://cdn.cboe.com/api/global/us_indices/governance/Volatility_Index_Methodology_Cboe_Volatility_Index.pd
Cboe SKEW Index White Paper is available at https://cdn.cboe.com/resources/indices/documents/SKEWwhitepaperjan2011.pdf.
Historical data for VIX come from https://www.cboe.com/tradable_products/vix/vix_historical_data/, and those for SKEW come from https://www.cboe.com/us/indices/dashboard/skew/.

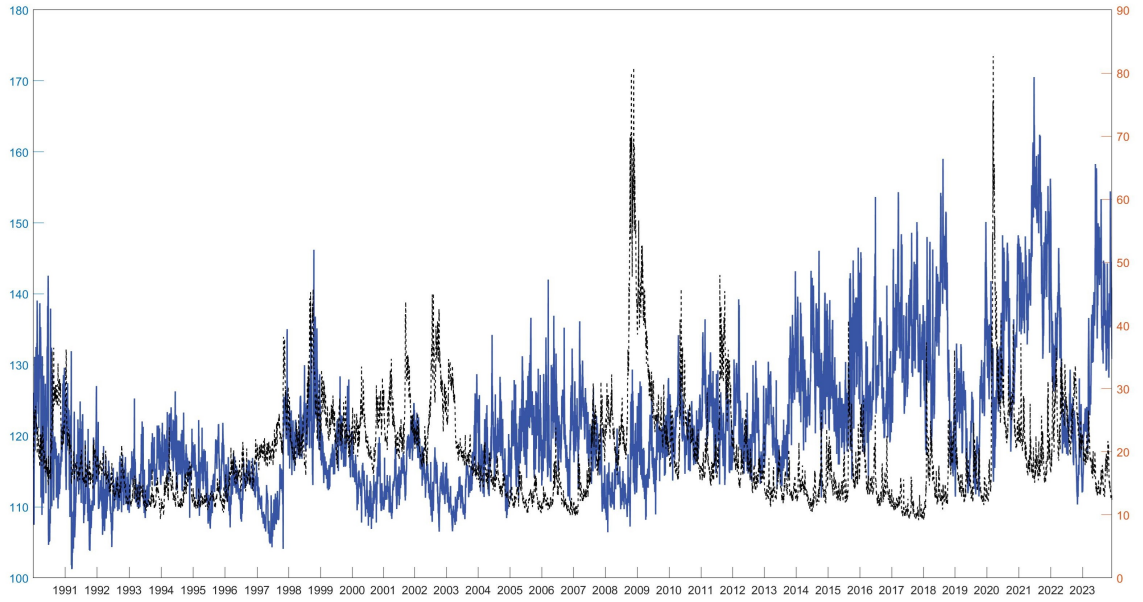

Figure 1: Dynamics of Skewness and Volatility

Notes: Figure 1 plots the daily time series of the Cboe SKEW Index (left axis) and the Cboe Volatility Index (right axis). SKEW is presented in blue solid line, and VIX is presented in black dashed line. This sample covers the period from January 2, 1990 to December 8, 2023, resulting in a total of 8,534 observations.

High-frequency intraday data are widely available, and any of realized measures is far more informative about the current level of variance than is the squared daily return (see Andersen et al. (2001a), Andersen et al. (2001b), Barndorff-Nielsen and Shephard (2002), Andersen et al. (2003), and Barndorff-Nielsen et al. (2008), among others). This makes realized measures very useful for modeling and forecasting variance of the underlying asset, and thus increasing option pricing accuracy. For example, Christoffersen et al. (2014), Christoffersen et al. (2015), Majewski et al. (2015), Huang et al. (2017), and Liang et al. (2023) show that incorporating realized variances in option valuation models improves option pricing performance. Moreover, realized skewness, as a measure of asymmetry constructed using high-frequency data, has been proposed to provide additional information on asset return distribution (see Feunou et al. (2016) and Feunou and Okou (2019) for example). The timely arrived information and accurate description of asymmetric behaviors of investors lead to better asset return forecasts (Amaya et al. (2015)).

To show the intraday pattern of skewness, Figure 2 plots the cumulative averaged 1-minute realized skewness of the S&P 500 index. Realized skewness is constructed following Feunou and Okou (2019). We find that the cumulative realized skewness exhibits a systematic intraday pattern,[2] rather than simply fluctuating around a specific level. Moreover, the occurrence of inflection points in the curve often coincides with macroeconomic releases, which sheds light on understanding intraday variations in stock return asymmetry. For example, changes in the direction of the curve might be triggered by ISM releases at 10:00 a.m. and FOMC announcements around 2:15 p.m., since these macroeconomic announcements are proved to have significant influence on equity markets (Lucca and Moench (2015) and Hu et al. (2022)). Intraday variations in stock return skewness underscore the need to incorporate high-frequency information using realized skewness measurements in volatility modeling and option pricing frameworks.

[2]The curve shows a rapid decline from market open to 10:00 a.m., followed by a moderate recovery reclaiming half of its value. Then the decline continues but decelerates, persisting until the window between 2:00 and 2:30 p.m. Interestingly, after 2:30 p.m., there is an ascent until the market close.

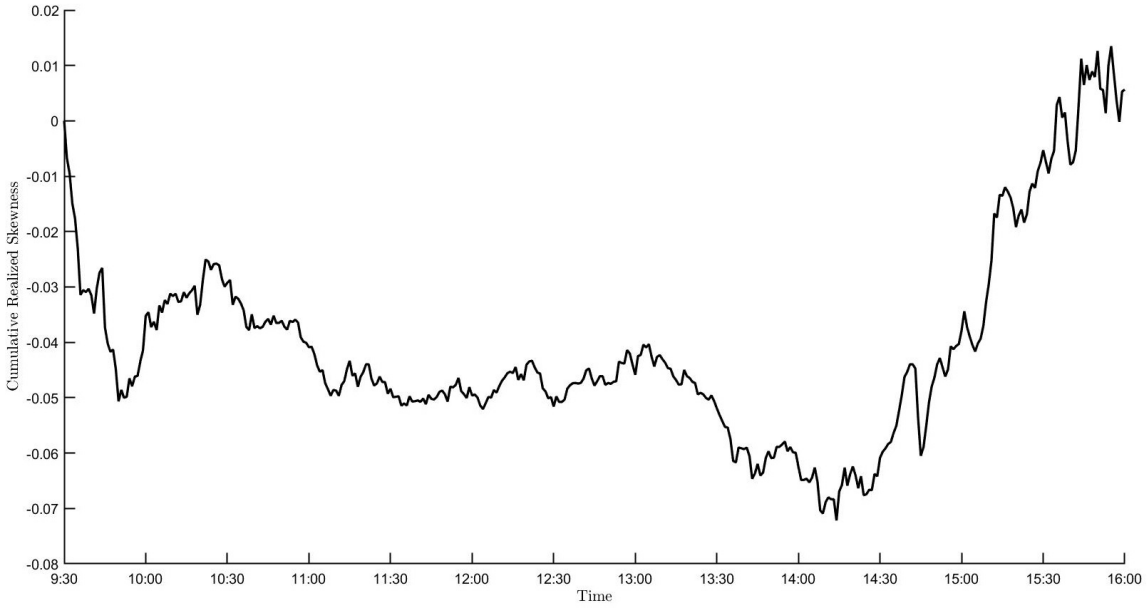

Figure 2: Intraday Pattern of Cumulative Realized Skewness: A Decline Followed by Recovery

Notes: Figure 2 plots the cumulative averaged 1-minute realized skewness of the S&P 500 index. We first compute intraday 1-minute returns, and 1-minute realized skewness (RS) measures are constructed following Feunou and Okou (2019). Then we obtain the averaged 1-minute RS values across trading days from May 1, 2007 to May 7, 2022, and plot the cumulative series from market open to close. RS values are annualized.

Building on these insights, this paper develops an option valuation model that allows dynamic conditional skewness in returns. We refer to this model as the Dynamic Conditional Skewness (DCS) model. The DCS model features different dynamics for conditional skewness and variance. To stress the difference in information, we use alternative realized measures constructed from high-frequency historical returns to update conditional skewness and variance. The affine structure of the new option pricing framework enables us to derive closed-form valuation formulas nesting popular specifications.

We find that explicitly modeling conditional skewness dynamics leads to substantial gains in option pricing. The new proposed DCS model effectively captures the historical and risk-neutral distributions of S&P 500 index returns. Specifically, when optimized on S&P 500 index options, realized measures, and returns, the DCS model achieves superior performance compared to nested

models and popular specifications. Overall, the joint modeling of dynamic conditional skewness and realized measures leads to an out-of-sample gain of 12.25% in pricing accuracy. The improvements are more pronounced for deep in-the-money calls, options with shorter maturities, and during highly volatile periods.

The main contribution of this paper is a new and flexible option pricing model that can accommodate different dynamics of skewness and variance in the underlying asset price process. Moreover, realized measures constructed from high-frequency data are proposed and used to update the dynamics, and any of these measures is far more informative about the current level of skewness and variance than is the daily return. The flexibility that the model offers for conditional skewness as well as timely arrived information from high-frequency data contribute to better variance and skewness forecasts, and thus to more accurate option prices.

The remainder of this paper is organized as follows. Section 2 introduces the new proposed option pricing models. Section 3 provides theoretical foundations and empirical implementations of realized components. Section 4 describes the physical estimation. In Section 5, we specify the risk-neutralization procedure and derive option valuation formula. We evaluate empirical option pricing performance in Section 6. Section 7 concludes.

2 The Model

This section develops an option pricing model that allows dynamic conditional asymmetries in returns. We refer to this model as the Dynamic Conditional Skewness (DCS) model. The DCS model features distinct dynamics and innovations for conditional skewness and conditional variance. Moreover, latent variables are updated using their model-free realized measures constructed from high-frequency historical returns on the underlying asset. Specifically, the model incorporates the information contained in returns (R_t), realized variances (RV_t), and realized skewness (RS_t). The flexibility that the model offers for conditional skewness as well as high-frequency information from the underlying asset may contribute to better variance and skewness forecasts, and thus to more accurate option prices.

The DCS model nests a parsimonious realized variance model as a special case, which we refer to as the Inverse Gaussian Affine Realized Volatility (IG-ARV) model. We propose the DCS model first, and the IG-ARV model is then developed in Section 2.2. The affine structure of the new option

pricing framework enables us to derive closed-form valuation formulas nesting popular specifications, which are discussed in Section 2.3.

2.1 The Dynamic Conditional Skewness Model

2.1.1 Asset Return Process

A. Asset Return Equation

We focus on the affine class of models (see Heston and Nandi (2000), Christoffersen et al. (2014), and Christoffersen et al. (2006), among others) where the exponentially affine moment generating function can be derived, and consider the following process for daily log returns:

$$R_{t+1} = r + \left(\lambda_z - \frac{1}{2}\right) h_t + (\lambda_y - \xi)\, s_t + \sqrt{h_t} z_{1,t+1} + \eta_1 y_{1,t+1}, \tag{1}$$

where r is the risk-free rate. h_t and s_t are latent variables that determine the dynamics of conditional variance and conditional skewness. λ_z and λ_y are compensations for volatility and skewness risk exposures. Next, we specify the conditional distribution of the total innovation $\sqrt{h_t} z_{1,t+1} + \eta_1 y_{1,t+1}$.

B. Innovation Conditional Distribution

Observed option biases, whereby out-of-the-money put prices and in-the-money call prices are relatively high compared to the Black-Scholes prices, are often represented by the "volatility smirk". Dynamic volatility models with Gaussian innovations capture these deviations from the Black–Scholes formula by incorporating conditional heteroskedasticity and including leverage parameters (see Heston and Nandi (2000), Chernov and Ghysels (2000), and Christoffersen and Jacobs (2004) for example). The combination of leverage parameters and conditional heteroskedasticity captures the leverage effect, that is, volatility increases relatively more when the stock price drops. This increases the probability of large losses, thereby increasing the value of the out-of-the-money put option. Equivalently, the implications of the leverage effect can be understood by recognizing that it generates negative skewness in stock returns.

Even with leverage parameters included, existing discrete-time models with Gaussian innovations are not sufficiently flexible to explain observed option biases (Christoffersen et al. (2006)). This is particularly the case for options with short maturities. While the leverage parameter generates negative skewness in multi-period returns, single-period innovations are Gaussian distributed,

and thus models with Gaussian innovations are not able to explain the biases in options with short maturities.

On this basis, we propose to include innovations to returns using a distribution with non-zero third-order conditional moments in addition to Gaussian innovations, thereby generating time-varying skewness in the return distribution and modeling its dynamics. To be more specific, we specify the total innovation, $\sqrt{h_t}z_{1,t+1} + \eta_1 y_{1,t+1}$, as a linear combination of a standard Gaussian innovation $z_{1,t+1}$ and an inverse Gaussian innovation $y_{1,t+1}$, and assume that Gaussian innovations are uncorrelated with inverse Gaussian innovations. The inverse Gaussian process has been investigated by Jensen and Lunde (2001), Forsberg and Bollerslev (2002), Christoffersen et al. (2006), and Feunou and Tédongap (2012). We consider the single-parameter inverse Gaussian distribution, $y_{1,t+1}|\mathcal{F}_t \sim IG(s_t)$, where s_t is the time-varying degree of freedom parameter.

Figure 3 compares return histogram and innovation densities. The histogram is based on S&P 500 sample returns, and the densities are plotted based on their analytical expressions. The density curve of the total innovation, $\sqrt{h_t}z_{1,t+1} + \eta_1 y_{1,t+1}$, is presented in solid line. The density of a Gaussian innovation $z_{1,t+1}$ and that of a single-parameter inverse Gaussian innovation $y_{1,t+1}$ are shown in dashed line and dotted line, respectively.

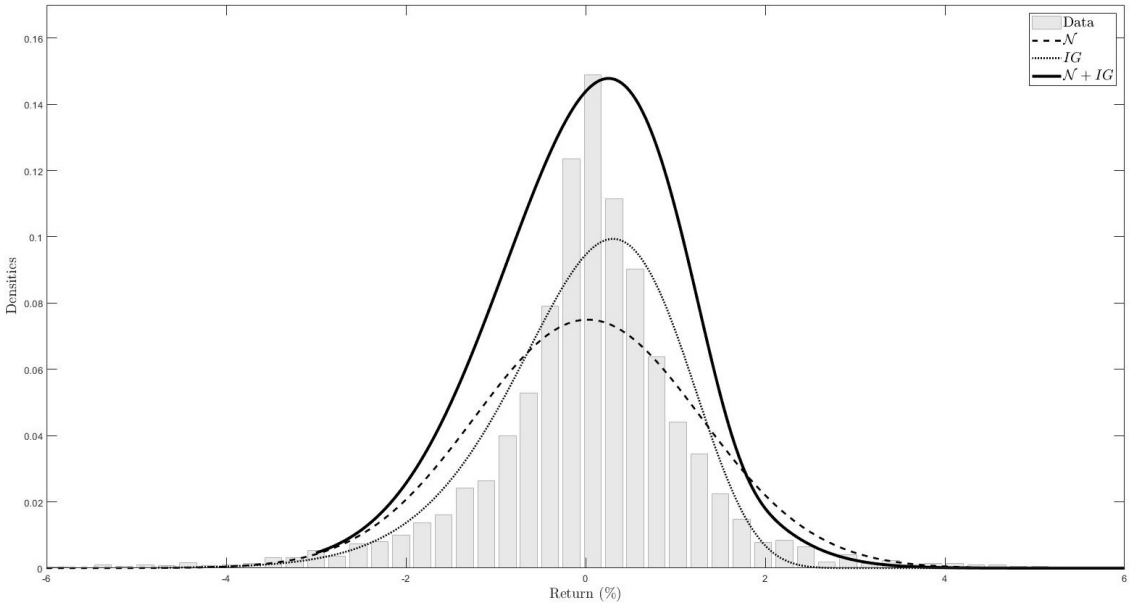

Figure 3: Return Histogram and Innovation Densities

Notes: Figure 3 makes a comparison of return histogram and innovation densities. The sample histogram covers the period from May 1, 2007 to May 7, 2022. We plot the Gaussian density with sample mean and sample variance in dashed line, the inverse Gaussian density with sample skewness in dotted line, and the density of a linear combination of the Gaussian innovation and the inverse Gaussian innovation $\sqrt{h}z + \eta y$ in solid line. h is set to sample variance and η matches sample skewness. Returns are in percentages.

We observe that the total innovation fits the sample distribution well, but the inverse Gaussian innovation fails to match the right tail of the sample density. As is evident in Figure 3, considering a linear combination of a standard Gaussian innovation and an inverse Gaussian innovation leads to a higher probability of large losses, thus increasing the value of out-of-the-money put options.

C. Return Conditional Moments

From Equation (1), the conditional expectation of R_{t+1},

$$\mathbb{E}_t\left[R_{t+1}\right] = r + \left(\lambda_z - \frac{1}{2}\right) h_t + \left(\lambda_y - \xi + \eta_1\right) s_t, \tag{2}$$

is a linear combination of latent variables h_t and s_t. The expected return is set up to satisfy the following equation:

$$\mathbb{E}_t\left[\exp\left(R_{t+1}\right)\right] = \exp\left(r + \lambda_z h_t + \lambda_y s_t\right), \tag{3}$$

and thus ξ is a particular function of η_1, $\xi = 1 - \sqrt{1 - 2\eta_1}$. Equation (3) enables us to interpret λ_z and λ_y as compensations for volatility and skewness risk exposures.

From the asset return equation, it is straightforward to obtain the conditional variance and conditional skewness based on properties of normal distribution and inverse Gaussian distribution.

$$\mathrm{Var}_t\left[R_{t+1}\right] = h_t + \eta_1^2 s_t. \tag{4}$$

From Equation (4), the dynamics of the conditional variance are completely determined by the dynamics of h_t and s_t. Furthermore, s_t has additional information content beyond the conditional variance for specifying the dynamics of the conditional skewness.

$$\mathrm{Skew}_t\left[R_{t+1}\right] = \frac{3\eta_1^3 s_t}{\mathrm{Var}_t\left[R_{t+1}\right]^{\frac{3}{2}}}. \tag{5}$$

2.1.2 Dynamic Equations

A. Dynamic Equation of h_t

Following Heston and Nandi (2000), Christoffersen et al. (2014), and Christoffersen et al. (2015), we will use the Gaussian shocks, $z_{2,t+1}$, to form a Gaussian shock conditional variance component of the form

$$h_{t+1} = \omega + \beta h_t + \alpha\left(z_{2,t+1} - \gamma\sqrt{h_t}\right)^2. \tag{6}$$

We allow for dependence between $z_{2,t+1}$ and daily return shocks $z_{1,t+1}$ by assuming they follow a bivariate standard normal distribution with correlation ρ,

$$\begin{pmatrix} z_{1,t+1} \\ z_{2,t+1} \end{pmatrix} \overset{i.i.d}{\sim} N\left(\begin{pmatrix} 0 \\ 0 \end{pmatrix}, \begin{pmatrix} 1 & \rho \\ \rho & 1 \end{pmatrix}\right). \tag{7}$$

From equation (6), γ captures the asymmetric volatility response, referred to as the leverage effect. Heston (1993) suggests that including a leverage parameter in option pricing models can enhance their performance by capturing the contemporaneous correlation between variance and return:

$$\mathrm{Cov}_t\left(R_{t+1}, h_{t+1}\right) = -2\alpha\gamma\rho h_t. \tag{8}$$

The leverage covariance of return and Gaussian shock conditional variance component is linear in h_t.

The subsequent moments implied by dynamic equation (6) will be crucial for comprehending the effectiveness of the DCS model in fitting returns, realized measures, and options. The expectation of Gaussian shock conditional variance component is represented as follows:

$$\mathbb{E}_t\left[h_{t+1}\right] = (\omega + \alpha) + \left(\beta + \alpha\gamma^2\right) h_t. \tag{9}$$

The conditional variance can be derived as

$$\mathrm{Var}_t\left[h_{t+1}\right] = 2\alpha^2\left(1 + 2\gamma^2 h_t\right), \tag{10}$$

which, like the leverage covariance in equation (8), is linear in h_t as well.

B. Dynamic Equation of s_t

We now need to specify the dynamics of s_t. The autoregressive coefficients of the corresponding realized measures $\widetilde{\mathrm{RS}}_t$ constructed from high-frequency historical returns suggest an AR(1) process:

$$s_{t+1} = w + bs_t + cy_{2,t+1}, \tag{11}$$

where $y_{2,t+1}$ has an inverse Gaussian conditional distribution with degrees of freedom parameter s_t, $y_{2,t+1}|\mathcal{F}_t \overset{i.i.d}{\sim} IG(s_t)$. As s_t is the conditional expectation in the IG distribution, $\mathbb{E}_t\left[y_{2,t+1}\right] = s_t$, the zero-mean innovation is given by $y_{2,t+1} - s_t$. Therefore, we rewrite equation (11) as

$$s_{t+1} = w + (b + c)\, s_t + c\left(y_{2,t+1} - s_t\right), \tag{12}$$

and impose $-1 < b + c < 1$ as the stationarity condition.

2.1.3 Measurement Equations

Each trading day, realized measures, $\widetilde{\mathrm{RV}}$ and $\widetilde{\mathrm{RS}}$, constructed from high-frequency intraday returns provide newly arrived information about latent variables, h and s. However, $\widetilde{\mathrm{RV}}$ and $\widetilde{\mathrm{RS}}$ are measured with error, and therefore, we specify the following measurement equations to describe the measurement relationships between latent variables and their corresponding empirical proxies. Theoretical foundations and empirical implementations of $\widetilde{\mathrm{RV}}$ and $\widetilde{\mathrm{RS}}$ are detailed in Section 3.

Following Christoffersen et al. (2014), we have a Gaussian distributed variable $z_{2,t+1}$ to capture the measurement error between the Gaussian shock conditional variance component h and its observed measure $\widetilde{\text{RV}}$,

$$\widetilde{\text{RV}}_{t+1} = h_t + \sigma \left[\left(z_{2,t+1} - \gamma \sqrt{h_t} \right)^2 - \left(1 + \gamma^2 h_t \right) \right]. \tag{13}$$

By construction, we have $\mathbb{E}_t \left[\widetilde{\text{RV}}_{t+1} \right] = h_t$. Equation (6) and equation (13) imply that h_t follows an AR(1) process. Meanwhile, the measurement error between the inverse Gaussian shock component s and its realized measure $\widetilde{\text{RS}}$ is naturally described by the inverse Gaussian innovation $y_{2,t+1}$,

$$\widetilde{\text{RS}}_{t+1} = s_t + d \left(y_{2,t+1} - s_t \right). \tag{14}$$

The innovation term inside the brackets in equation (14), $y_{2,t+1} - s_t$, is constructed to have zero mean ensuring that $\mathbb{E}_t \left[\widetilde{\text{RS}}_{t+1} \right] = s_t$.

In Section 4, we will be estimating the model using standard Quasi Maximum Likelihood Estimation (QMLE). We have observations on R, $\widetilde{\text{RV}}$, and $\widetilde{\text{RS}}$, and for estimation, we need to derive their conditional moments implied by the model. We have already provided $\mathbb{E}_t \left[R_{t+1} \right]$, $\text{Var}_t \left[R_{t+1} \right]$, $\mathbb{E}_t \left[\widetilde{\text{RV}}_{t+1} \right]$, and $\mathbb{E}_t \left[\widetilde{\text{RS}}_{t+1} \right]$ above. In addition, we need the conditional variance of $\widetilde{\text{RV}}$,

$$\text{Var}_t \left[\widetilde{\text{RV}}_{t+1} \right] = 2\sigma^2 \left(1 + 2\gamma^2 h_t \right), \tag{15}$$

and the conditional variance of $\widetilde{\text{RS}}_{t+1}$,

$$\text{Var}_t \left[\widetilde{\text{RS}}_{t+1} \right] = d^2 s_t. \tag{16}$$

We refer to this general specification as the Dynamic Conditional Skewness (DCS) model. The DCS model has 13 parameters[3] in total, and it may prove useful to also investigate a more parsimonious special case where only the RV component plays a role in the conditional skewness dynamic. We now develop such a model, which we refer to as the Inverse Gaussian Affine Realized Volatility (IG-ARV) model.

2.2 The Inverse Gaussian Affine Realized Volatility Model

In practice, it may be helpful to use a more parsimonious model that still allows for time-varying conditional skewness and has an analytical option pricing formula. We refer to this model as

[3] In subsequent empirics, we apply variance targeting technique, and thus ω is set to match sample variance, meanwhile w is set to match sample skewness. Therefore, there are 11 parameters to be estimated.

the Inverse Gaussian Affine Realized Volatility (IG-ARV) model. In the IG-ARV model, realized variances RV calculated from high-frequency intraday returns are incorporated to update the conditional variance dynamics with new arrived information, and the dynamics of conditional skewness can be derived from the dynamics of conditional variance. We also provide measurement equation to describe the measurement relationship between conditional variance h^{RV} and its corresponding realized measure RV.

We combine the non-zero conditional skewness of the inverse Gaussian distribution with ARV dynamics (Christoffersen et al. (2014)) where RV is used to construct today's spot volatility. This gives the model flexibility to generate time-varying skewness in the return distribution and obtain more accurate estimates of volatility and skewness.

The new stock return dynamic is specified as

$$R_{t+1} = r + v h_t^{\text{RV}} + \eta y_{1,t+1}, \tag{17}$$

where, given the available information at time t, $y_{1,t+1}$ has an inverse Gaussian conditional distribution $y_{1,t+1}|\mathcal{F}_t \sim IG(\delta_t)$ with degrees of freedom parameter $\delta_t = h_t^{\text{RV}}/\eta^2$. Therefore, we can use the properties of inverse Gaussian distribution to calculate conditional variance and conditional skewness,

$$\text{Var}_t\left[R_{t+1}\right] = h_t^{\text{RV}}, \tag{18}$$

$$\text{Skew}_t\left[R_{t+1}\right] = 3\eta\left(h_t^{\text{RV}}\right)^{-\frac{1}{2}}. \tag{19}$$

Note that, like the IG GARCH model (Christoffersen et al. (2006)), the conditional skewness in the IG-ARV model is also determined by the conditional variance. Thus, we are able to derive the model implied dynamics of conditional skewness. The conditional variance dynamic of return is specified as,

$$h_{t+1}^{\text{RV}} = w + b h_t^{\text{RV}} + c y_{2,t+1} + a\frac{\left(h_t^{\text{RV}}\right)^2}{y_{2,t+1}}, \tag{20}$$

where $y_{2,t+1}|\mathcal{F}_t \sim IG(\delta_t)$ and $\text{Corr}_t(y_{1,t+1}, y_{2,t+1}) = 0$.

The corresponding measurement equation is given by

$$\text{RV}_{t+1} = h_t^{\text{RV}} + d\left[c y_{2,t+1} + a\frac{\left(h_t^{\text{RV}}\right)^2}{y_{2,t+1}} - \left(\left(\frac{c}{\eta^2} + a\eta^2\right)h_t^{\text{RV}} + a\eta^4\right)\right], \tag{21}$$

where $\mathbb{E}_t\left[\text{RV}_{t+1}\right] = h_t^{\text{RV}}$.

2.3 Nested Models

Before the empirical estimation, we discuss special cases of interest that are nested by new proposed option pricing models. In the following empirical studies, we compare the performance of the DCS model and the IG-ARV model to these nested specifications and popular benchmarks.

2.3.1 The Affine Realized Volatility Model

According to Wald (1947), as the degree of freedom parameter $\delta \to \infty$, the standardized inverse Gaussian distribution converges to an asymptotic Gaussian distribution. Therefore, the IG-ARV model is closely related to existing GARCH processes. Specifically, for a finite h^{RV}, by taking the limit as $\eta \to 0$ and using the following parameterization:

$$\begin{aligned} v &= \lambda - \frac{1}{\eta}, \\ a &= \frac{\alpha}{\eta^4}, \\ w &= \omega, \\ c &= \alpha - 2\alpha\gamma\eta, \\ b &= \beta + \alpha\gamma^2 - \frac{2\alpha}{\eta^2} + \frac{2\alpha\gamma}{\eta}, \\ d &= \frac{\alpha}{\sigma}, \end{aligned} \tag{22}$$

the IG-ARV model converges to the Affine Realized Volatility (ARV) model in Christoffersen et al. (2014) with Gaussian innovations $\varepsilon_{1,t+1}$ and $\varepsilon_{2,t+1}$:

$$\begin{aligned} R_{t+1} &= r + \lambda h_t^{\mathrm{RV}} - \frac{1}{2} h_t^{\mathrm{RV}} + \sqrt{h_t^{\mathrm{RV}}}\varepsilon_{1,t+1}, \\ h_{t+1}^{\mathrm{RV}} &= \omega_2 + \beta_2 h_t^{\mathrm{RV}} + \alpha_2 \left(\varepsilon_{2,t+1} - \gamma_2 \sqrt{h_t^{\mathrm{RV}}}\right)^2, \\ \mathrm{RV}_{t+1} &= h_t^{\mathrm{RV}} + \sigma \left[\left(\varepsilon_{2,t+1} - \gamma_2 \sqrt{h_t^{\mathrm{RV}}}\right)^2 - \left(1 + \gamma_2^2 h_t^{\mathrm{RV}}\right) \right]. \end{aligned} \tag{23}$$

It can be shown that the parameterization in equation (22) matches the first two conditional moments of the IG-ARV model with those in the ARV model.

Proof: See Appendix A. ■

2.3.2 The Inverse Gaussian GARCH Model

The realized measurements constructed by high-frequency data are used to inform the IG-ARV model about time variation in conditional variance. Furthermore, if the dynamics of the conditional variance are driven by daily observables, then we obtain the Inverse Gaussian GARCH (IG GARCH) model (Christoffersen et al. (2006)):

$$R_{t+1} = r + vh_{t+1} + \eta y_{t+1}, \tag{24}$$

$$h_{t+1} = w + bh_t + cy_t + a\frac{h_t^2}{y_t}, \tag{25}$$

where the degree of freedom parameter $\delta_{t+1} = \frac{h_{t+1}}{\eta^2}$.

2.3.3 The Heston-Nandi GARCH Model

As the degree of freedom parameter approaches infinity, the standardized inverse Gaussian distribution converges to an asymptotic Gaussian distribution. Therefore, the relationship between the IG GARCH model and the Heston-Nandi GARCH (HNG) model (Heston and Nandi (2000)) is similar to the relationship between the IG-ARV model and the ARV model. Again, by taking the limit as $\eta \to 0$ and using the parameterization (except for the last equation) presented in equation (22), we can obtain the HNG model:

$$\begin{aligned} R_{t+1} &= r + \lambda h_t - \frac{1}{2}h_t + \sqrt{h_t}\varepsilon_{t+1}, \\ h_{t+1} &= \omega_2 + \beta_2 h_t + \alpha_2 \left(\varepsilon_{t+1} - \gamma\sqrt{h_t}\right)^2. \end{aligned} \tag{26}$$

Similarly, the parameterization used above matches the first two conditional moments of the IG GARCH model with those in the HNG model.

3 Realized Components

In this section, we first briefly review the theoretical results that allow us to separate daily upside from downside variance using intraday data and measure skewness by the relative semi-variance. On this basis, we then construct realized measures of Gaussian variation component and IG component, plot daily realized variation component series along with daily returns, and investigate their dynamics.

3.1 Measuring Realized Skewness: Theoretical Foundations

Barndorff-Nielsen et al. (2008) assume that the log stock price Y follows a jump-diffusion motion of the form

$$dY_t = \mu_t dt + \sigma_t dW_t + \Delta Y_t, \tag{27}$$

where W_t is a standard Brownian motion, and ΔY_t is a jump process in Y as $\Delta Y_t = Y_t - Y_{t-}$.

According to Feunou et al. (2016) and Feunou and Okou (2019), for a unimodal distribution of log returns, the relative magnitude of upside and downside variance can be perceived as a measure of asymmetry. For daily log return R following a unimodal distribution, denote the upside variance as

$$\sigma_u^2 = \mathrm{Var}[R \mid R > 0], \tag{28}$$

and the downside variance as

$$\sigma_d^2 = \mathrm{Var}[R \mid R \leq 0]. \tag{29}$$

Then, the total variance is

$$\sigma^2 = \mathrm{Var}[R] = \sigma_u^2 \cdot \mathrm{Prob}(R > 0) + \sigma_d^2 \cdot \mathrm{Prob}(R \leq 0). \tag{30}$$

Following Andersen et al. (2003) and Barndorff-Nielsen et al. (2008), the corresponding realized measures of the upside variance, the downside variance, and the total variance are respectively given by

$$\mathrm{RV}_t^U = \sum_{j=1}^{n_t} R_{t_j}^2 \mathbb{I}_{\left[R_{t_j} > 0\right]}, \tag{31}$$

$$\mathrm{RV}_t^D = \sum_{j=1}^{n_t} R_{t_j}^2 \mathbb{I}_{\left[R_{t_j} \leq 0\right]}, \tag{32}$$

$$\mathrm{RV}_t = \mathrm{RV}_t^U + \mathrm{RV}_t^D, \tag{33}$$

where $R_{t_j} = Y_{t_j} - Y_{t_{j-1}}$, $t - 1 < t_1 < \cdots < t_{n_t} = t$. $\mathbb{I}$ is the indicator function. Under the general assumption on the return process in equation (27), Barndorff-Nielsen et al. (2008) prove that

$$\begin{aligned} \mathrm{RV}_t^U &\xrightarrow{p} \frac{1}{2}\int_{t-1}^{t} \sigma_v^2 dv + \sum_{t-1 \leq v \leq t} (\Delta Y_v)^2 \mathbb{I}_{[\Delta Y_v > 0]}, \\ \mathrm{RV}_t^D &\xrightarrow{p} \frac{1}{2}\int_{t-1}^{t} \sigma_v^2 dv + \sum_{t-1 \leq v \leq t} (\Delta Y_v)^2 \mathbb{I}_{[\Delta Y_v \leq 0]}. \end{aligned} \tag{34}$$

The distribution is right-skewed if $\sigma_u^2 > \sigma_d^2$, and left-skewed if $\sigma_u^2 < \sigma_d^2$. Therefore, the difference between upside and downside variance, the relative semi-variance, provides a non-parametric and distribution-free measure for conditional skewness in returns:

$$\text{RSV} \equiv \sigma_u^2 - \sigma_d^2. \tag{35}$$

A theoretical justification for using the relative semi-variance as a measure of conditional skewness is given by Feunou et al. (2016). The corresponding realized skewness measure is obtained by

$$\text{RSV}_t = \text{RV}_t^U - \text{RV}_t^D. \tag{36}$$

To provide asymptotic intuition on RSV_t for further discussion, we combine equation (34) and equation (36) to get

$$\text{RSV}_t \xrightarrow{p} \sum_{t-1 \leq v \leq t} (\Delta Y_v)^2 \left(\mathbb{I}_{[\Delta Y_v > 0]} - \mathbb{I}_{[\Delta Y_v \leq 0]} \right). \tag{37}$$

3.2 Constructing Realized Components: Empirical Implementations

We use intraday S&P 500 index (SPX) data to empirically construct realized variance components. The historical high-frequency data are obtained from FirstRate Data. The sample period is from May 1, 2007 to May 7, 2022. Data are sampled at the end of each 5-minute interval.

On trading day t, we compute 5-minute SPX log returns R_{t_j} using the last tick in each 5-minute interval. The close-to-open log return $R_{CO,t}$ is

$$R_{CO,t} = Y_{O,t} - Y_{t-1},$$

where $Y_{O,t}$ is the opening log price on trading day t. Following Andersen et al. (2003), Barndorff-Nielsen et al. (2008), and Feunou and Okou (2019), we compute realized upside variance, realized downside variance, and total realized variance as

$$\begin{aligned}
\text{RV}_t^U &= R_{CO,t}^2 \mathbb{I}_{[R_{CO,t} > 0]} + \sum_{j=1}^{n_t} R_{t_j}^2 \mathbb{I}_{\left[R_{t_j} > 0\right]}, \\
\text{RV}_t^D &= R_{CO,t}^2 \mathbb{I}_{[R_{CO,t} \leq 0]} + \sum_{j=1}^{n_t} R_{t_j}^2 \mathbb{I}_{\left[R_{t_j} \leq 0\right]}, \\
\text{RV}_t &= R_{CO,t}^2 + \sum_{j=1}^{n_t} R_{t_j}^2 = \text{RV}_t^U + \text{RV}_t^D.
\end{aligned} \tag{38}$$

To ensure that the sample mean of the daily total realized variances is equal to the sample variance of the daily log returns, we also perform the scaling method in Feunou and Okou (2019). Specifically, we use the scale factor

$$\frac{\sum_{t=1}^{T}\left(R_t-\bar{R}_T\right)^2}{\sum_{t=1}^{T}\mathrm{RV}_t}$$

to adjust realized variance measures in equation (38), where T denotes the sample size, and $\bar{R}_T$ is the sample mean of the daily log returns.

Now we are ready to compute realized skewness RSV_t in equation (36) using scaled realized upside and downside variances, and the asymptotic limit is given by equation (37). From the two equations, RSV_t shows how likely positive jumps are relative to negative jumps. Feunou et al. (2016) have observed that in data sampled at high enough frequency (for example, the 5-minute sampling frequency in this study), conditional skewness is driven purely by jumps.[4] Thus, RSV_t shows how likely the return asymmetry occurs. Furthermore, from equation (37), the relative possibility (or the direction) of jumps receive weights according to realized jump sizes. Therefore, RSV_t measures the possibility and magnitude of asymmetry in returns.

In the DCS model, the return asymmetry is entirely determined by the realization of inverse Gaussian innovation $y_{1,t+1}|\mathcal{F}_t \sim IG(s_t)$, where $s_t = \mathbb{E}_t\left[y_{1,t+1}\right]$ is the conditional expectation of $y_{1,t+1}$. Therefore, the absolute value of $\mathrm{RSV_t}$ capturing the magnitude of asymmetry in returns provides a realized measure of s_t:

$$\widetilde{\mathrm{RS}}_t = |\mathrm{RSV}_t| = \begin{cases} \mathrm{RV}_t^U - \mathrm{RV}_t^D, & \mathrm{RV}_t^U > \mathrm{RV}_t^D \\ \mathrm{RV}_t^D - \mathrm{RV}_t^U, & \mathrm{RV}_t^U \leq \mathrm{RV}_t^D. \end{cases} \tag{39}$$

Moreover, the conditional variance in the DCS model consists of two components, Gaussian variation component h_t and IG component s_t. On this basis, we then obtain a realized measure of h_t by subtracting $\widetilde{\mathrm{RS}}_t$ from the realized variance:

$$\widetilde{\mathrm{RV}}_t = \mathrm{RV}_t - \widetilde{\mathrm{RS}}_t. \tag{40}$$

3.3 Dynamics of Historical Realized Components

Figure 4 plots daily time series of realized components of S&P 500 index, following the construction methodology in Section 3.2. Graph A presents daily returns (R_t), and realized components, $\sqrt{\widetilde{\mathrm{RV}}_t}$

[4] According to Feunou et al. (2016), this assumption is reasonable at frequencies including 5-minute, 15-minute, half-hour, hourly, and even daily, since the instantaneous leverage effect is weak enough at such high frequencies.

and $\sqrt{\widetilde{\mathrm{RS}}_t}$, are shown in Graph B and C, respectively. The sample period is from May 1, 2007 to May 7, 2022.

We could see large swings in returns and high level of $\widetilde{\mathrm{RV}}_t$ during 2008 financial crisis. Moreover, Graph B and C not only display synchronicity, but also show different dynamic patterns and evolution tracks of $\widetilde{\mathrm{RV}}_t$ and $\widetilde{\mathrm{RS}}_t$. For example, the peak of historical series of $\widetilde{\mathrm{RS}}_t$ appears in 2020. The intraday price evolution follows a specific direction, reflecting more unified market sentiment, therefore, intraday returns are more skewed on that trading day. Thus, as a higher-order measure, $\widetilde{\mathrm{RS}}_t$ incorporates different market implications and additional information content beyond the variance series that may contribute to better skewness forecasts, and thus more accurate option prices.

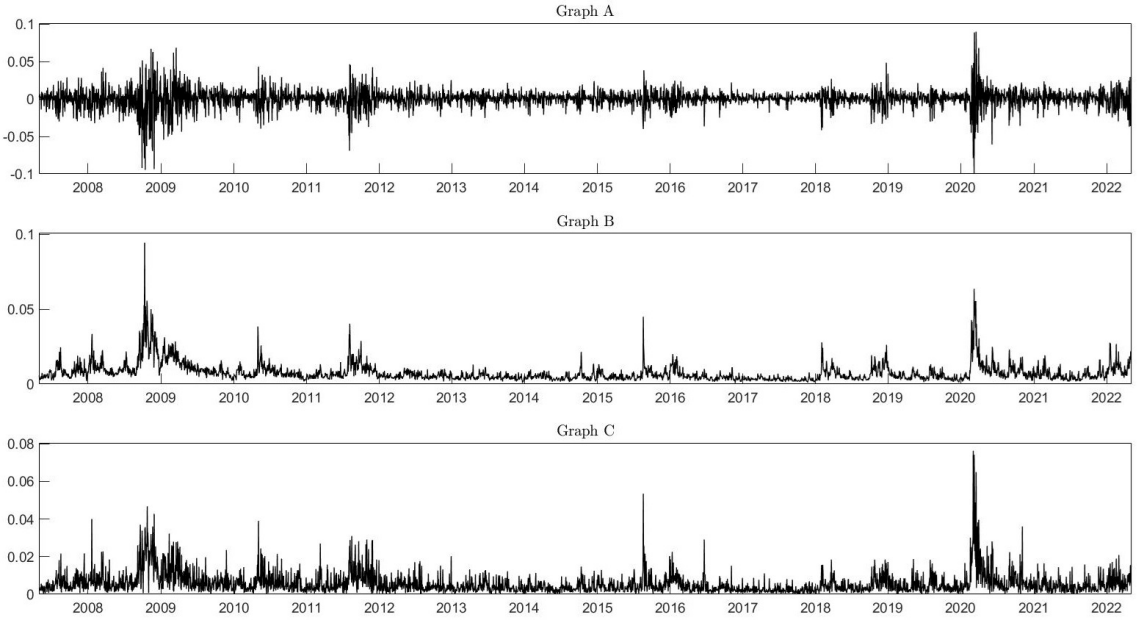

Figure 4: Historical Series of Returns and Realized Components

Notes: Figure 4 presents daily returns (R_t) of the S&P 500 index in Graph A, and realized components ($\sqrt{\widetilde{\mathrm{RV}}_t}$ and $\sqrt{\widetilde{\mathrm{RS}}_t}$) in Graph B and C. $\widetilde{\mathrm{RV}}_t$ and $\widetilde{\mathrm{RS}}_t$ are constructed based on the methodology described in Section 3.2. The sample starts on May 1, 2007 and ends on May 7, 2022.

To show the dynamic behaviors of returns and realized components, Figure 5 plots their autocorrelation functions (ACFs) for lags 1 through 60. The horizontal lines mark a Bartlett two-standard-

error confidence interval around 0. Daily returns are negatively correlated with one-period lags and exhibit little persistence associated with higher lags. Both of the realized variance components are highly persistent, capturing volatility clustering. Specifically, the ACF of $\widetilde{\mathrm{RV}}_t$ remains significant when lag reaches 60. Moreover, $\widetilde{\mathrm{RS}}_t$ is also quite persistent, providing evidence for the dynamics of s_t.

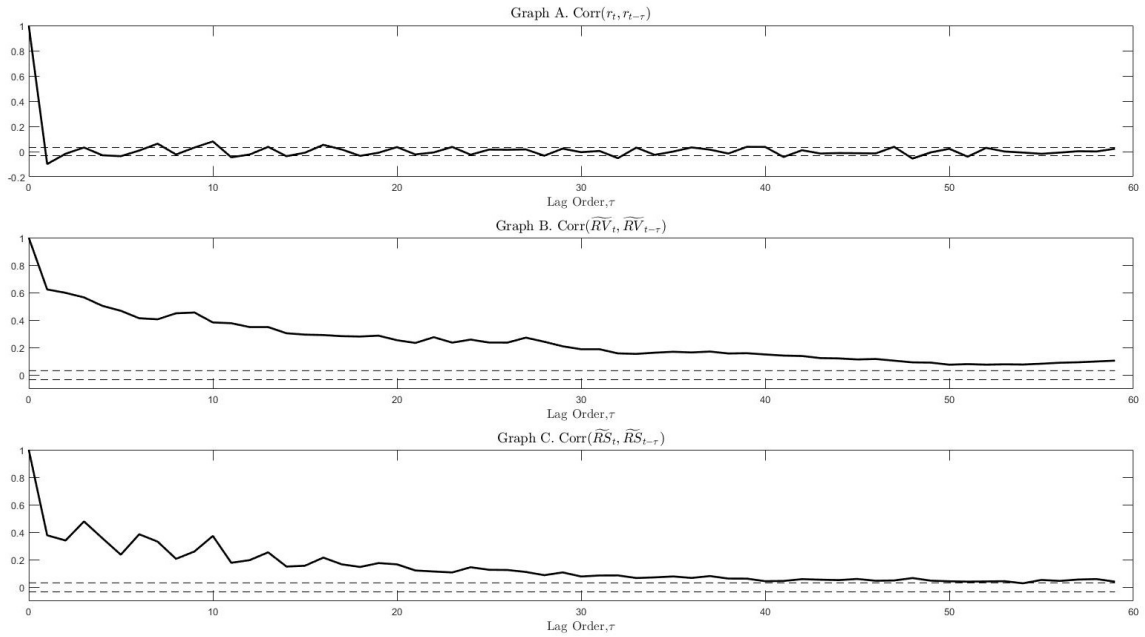

Figure 5: Autocorrelations of Returns and Realized Components

Notes: Figure 5 presents the autocorrelations of daily returns (R_t) of the S&P 500 index in Graph A, and daily realized components ($\widetilde{\mathrm{RV}}_t$ and $\widetilde{\mathrm{RS}}_t$) in Graph B and C. In each graph, lag orders between 1 and 60 trading days are used. The horizontal lines mark Bartlett ±2-standard-error bands. The sample starts on May 1, 2007 and ends on May 7, 2022.

Table 1 reports summary statistics of daily returns and realized components. The skewness of sample returns is -0.6304, indicating that the sample distribution of return is left-skewed. Therefore, we expect a negative estimate of η in the DCS model. Moreover, both of the realized components are highly persistent, with AR(1) coefficient of 0.9235 and 0.7132, respectively, and this is consistent with the results in Figure 5. The above findings are in line with existing studies such as Christoffersen et al. (2006) and Feunou and Okou (2019).

Table 1: Summary Statistics of Returns and Realized Components

Summary Statistics of Returns and Realized Components

Series	Mean	Median	Std. Dev.	Skewness	Kurtosis	AR(1)
Return	6.2593	17.8615	20.0178	-0.6304	12.1613	-0.0982
Gaussian Component	11.9142	9.1275	9.6907	3.7793	28.1801	0.9235
IG Component	8.9986	6.3395	9.1553	3.5789	26.4633	0.7132

Notes: Table 1 reports summary statistics of return (R_t), the square root of Gaussian realized variance component ($\sqrt{\widetilde{\mathrm{RV}}_t}$), and the square root of IG realized variance component ($\sqrt{\widetilde{\mathrm{RS}}_t}$). Sample mean, median, and standard deviation are annualized and presented in percentages. AR(1) denotes the first-order autocorrelation coefficient. The sample starts on May 1, 2007 and ends on May 7, 2022.

4 Estimation on the Underlying Asset

In this section, we use the quasi maximum likelihood estimation method to estimate model parameters using daily observations on returns, as well as the realized components constructed in Section 3.

4.1 Quasi Maximum Likelihood Estimation

Because $\mathrm{Corr}_t(z_{1,t+1}, y_{2,t+1}) = 0$, $\mathrm{Corr}_t(y_{1,t+1}, y_{2,t+1}) = 0$, and $\mathrm{Corr}_t(z_{2,t+1}, y_{2,t+1}) = 0$, the conditional joint probability density function (PDF) of returns and realized components can be written as

$$f_t\left(R_{t+1}, \widetilde{\mathrm{RV}}_{t+1}, \widetilde{\mathrm{RS}}_{t+1}\right) = f_t\left(R_{t+1}, \widetilde{\mathrm{RV}}_{t+1}\right) \cdot f_{s,t}\left(\widetilde{\mathrm{RS}}_{t+1}\right). \tag{41}$$

Further, the Sklar's theorem implies that

$$f_t\left(R_{t+1}, \widetilde{\mathrm{RV}}_{t+1}\right) = f_{r,t}\left(R_{t+1}\right) \cdot f_{h,t}\left(\widetilde{\mathrm{RV}}_{t+1}\right) \cdot c_t\left(F_{r,t}\left(R_{t+1}\right), F_{h,t}\left(\widetilde{\mathrm{RV}}_{t+1}\right)\right), \tag{42}$$

where $f_{r,t}\left(R_{t+1}\right)$, $f_{h,t}\left(\widetilde{\mathrm{RV}}_{t+1}\right)$, and $f_{s,t}\left(\widetilde{\mathrm{RS}}_{t+1}\right)$ are conditional PDFs. $F_{r,t}\left(R_{t+1}\right)$ and $F_{h,t}\left(\widetilde{\mathrm{RV}}_{t+1}\right)$ are conditional cumulative distribution functions (CDFs). c_t is the conditional copula density. Plug

Equation (42) into Equation (41) and take the logarithm, we have

$$\begin{aligned}\log f_t\left(R_{t+1}, \widetilde{\mathrm{RV}}_{t+1}, \widetilde{\mathrm{RS}}_{t+1}\right) = &\log f_{r,t}\left(R_{t+1}\right) + \log f_{h,t}\left(\widetilde{\mathrm{RV}}_{t+1}\right) + \log f_{s,t}\left(\widetilde{\mathrm{RS}}_{t+1}\right) \\ &+ \log c_t\left(F_{r,t}\left(R_{t+1}\right), F_{h,t}\left(\widetilde{\mathrm{RV}}_{t+1}\right)\right).\end{aligned} \tag{43}$$

Because $\mathrm{Corr}_t(y_{1,t+1}, z_{2,t+1}) = 0$ and

$$\begin{pmatrix} z_{1,t+1} \\ z_{2,t+1} \end{pmatrix} \overset{i.i.d}{\sim} N\left(\begin{pmatrix} 0 \\ 0 \end{pmatrix}, \begin{pmatrix} 1 & \rho \\ \rho & 1 \end{pmatrix}\right),$$

we follow Feunou and Okou (2019) and specify c_t as a Gaussian copula.

Now we are ready to derive the quasi-log-likelihood function. Firstly, the quasi-log-likelihood of $\widetilde{\mathrm{RV}}$ at time $t+1$ conditional on information at time t is

$$\log l_{h,t}\left(\widetilde{\mathrm{RV}}_{t+1}\right) = -\frac{1}{2}\log\left(2\pi\right) - \frac{1}{2}\log\left(\mathrm{Var}_t\left[\widetilde{\mathrm{RV}}_{t+1}\right]\right) - \frac{\left(\widetilde{\mathrm{RV}}_{t+1} - h_t\right)^2}{2\,\mathrm{Var}_t\left[\widetilde{\mathrm{RV}}_{t+1}\right]}, \tag{44}$$

where $\mathrm{Var}_t\left[\widetilde{\mathrm{RV}}_{t+1}\right]$ is given in Equation (15). The conditional CDF of $\widetilde{\mathrm{RV}}$ is

$$F_{h,t}\left(\widetilde{\mathrm{RV}}_{t+1}\right) = \Phi\left(\frac{\widetilde{\mathrm{RV}}_{t+1} - h_t}{\sqrt{\mathrm{Var}_t\left[\widetilde{\mathrm{RV}}_{t+1}\right]}}\right), \tag{45}$$

where $\Phi(\cdot)$ is the CDF of a standard normal distribution.

Based on the inverse Gaussian density, the log-likelihood function of $\widetilde{\mathrm{RS}}$ is given by

$$\log l_{s,t}\left(\widetilde{\mathrm{RS}}_{t+1}\right) = -\frac{1}{2}\log\left(2\pi\right) - \log\left(\left|\widetilde{\mathrm{RS}}_{t+1} - (1-d)\,s_t\right|\right) + \log\left(-\frac{Y_{1,t}+Y_{2,t}}{2}\right) - \frac{1}{2}Y_{1,t}^2, \tag{46}$$

where $Y_{1,t}$ and $Y_{2,t}$ are components in the inverse Gaussian density:

$$Y_{1,t} = \sqrt{\frac{\widetilde{\mathrm{RS}}_{t+1} - (1-d)\,s_t}{d}} - \frac{s_t}{\sqrt{\frac{\widetilde{\mathrm{RS}}_{t+1} - (1-d)s_t}{d}}}, \tag{47}$$

$$Y_{2,t} = -\sqrt{\frac{\widetilde{\mathrm{RS}}_{t+1} - (1-d)\,s_t}{d}} - \frac{s_t}{\sqrt{\frac{\widetilde{\mathrm{RS}}_{t+1} - (1-d)s_t}{d}}}. \tag{48}$$

To emphasize the asymmetry of the conditional distribution of returns, we need the exact PDF, $f_{r,t}\left(R_{t+1}\right)$. Note that the innovation term in the asset return process is a linear combination,

$\sqrt{h_t}z_{1,t+1}+\eta_1 y_{1,t+1}$, where $z_{1,t+1} \overset{i.i.d}{\sim} \mathcal{N}(0,1)$ and $y_{1,t+1} \overset{i.i.d}{\sim} IG(s_t)$. Thus, the PDF of returns does not have an existing closed-form expression. Nonetheless, the closed-form conditional characteristic function of R_{t+1} is available:

$$\begin{aligned}\varphi_{r,t}(\nu) &\equiv \mathbb{E}_t\left[e^{i\nu R_{t+1}}\right] \\ &= \exp\left(i\nu r + \left(i\nu\lambda_z - \frac{1}{2}i\nu - \frac{1}{2}\nu^2\right)h_t + \left(i\nu\left(\lambda_y - \xi\right) + 1 - \sqrt{1-2\eta_1 i\nu}\right)s_t\right),\end{aligned} \tag{49}$$

where i denotes the imaginary unit. Therefore, we use Fourier inversion to obtain $F_{r,t}\left(R_{t+1}\right)$ and $f_{r,t}\left(R_{t+1}\right)$:

$$F_{r,t}\left(R_{t+1}\right) = \frac{1}{2} - \frac{1}{\pi}\int_0^\infty \frac{\operatorname{Im}\left[e^{-i\nu R_{t+1}}\varphi_{r,t}(\nu)\right]}{\nu}d\nu, \tag{50}$$

$$f_{r,t}\left(R_{t+1}\right) = \frac{1}{\pi}\int_0^\infty \operatorname{Re}\left[e^{-i\nu R_{t+1}}\varphi_{r,t}(\nu)\right]d\nu. \tag{51}$$

In addition, the Gaussian copula function is given by

$$c_t\left(v, v_h\right) = \frac{1}{\sqrt{|\mathrm{CM}_t|}}\exp\left(-\frac{1}{2}\left(v, v_h\right)\left(\mathrm{CM}_t^{-1} - I_2\right)\begin{pmatrix} v \\ v_h \end{pmatrix}\right), \tag{52}$$

where CM_t denotes the conditional correlation matrix of $\left(R_{t+1}, \widetilde{\mathrm{RV}}_{t+1}\right)$, represented as

$$\mathrm{CM}_t = \begin{bmatrix} 1 & \rho_{h,t} \\ \rho_{h,t} & 1 \end{bmatrix}. \tag{53}$$

$\rho_{h,t}$ is the conditional correlation of R_{t+1} and $\widetilde{\mathrm{RV}}_{t+1}$, computed as

$$\rho_{h,t} = \frac{\mathrm{Cov}_t\left(R_{t+1}, \widetilde{\mathrm{RV}}_{t+1}\right)}{\sqrt{\mathrm{Var}_t\left[R_{t+1}\right]\mathrm{Var}_t\left[\widetilde{\mathrm{RV}}_{t+1}\right]}}. \tag{54}$$

Finally, we obtain the sample log-likelihood function by summing the log likelihoods over all the observations:

$$\mathcal{L}^P = \sum_{t=1}^{T-1}\log l_t\left(R_{t+1}, \widetilde{\mathrm{RV}}_{t+1}, \widetilde{\mathrm{RS}}_{t+1}\right). \tag{55}$$

The log-likelihood is an aggregate measure of fit, reflecting the combined contributions from returns and realized components.

4.2 Estimation Results

Table 2 reports the estimation results under $\mathbb{P}$ measure. The dataset comprises daily returns and realized measures of the S&P 500 index, covering the period from May 1, 2007 to May 7, 2022. We compare the newly proposed models with nested specifications discussed in Section 2.3. Specifically, the DCS model is estimated on realized components ($\widetilde{\text{RV}}$ and $\widetilde{\text{RS}}$) constructed in Section 3 and daily returns. The IG-ARV model and the ARV model are estimated using realized variances and daily returns. The IG GARCH model and the HNG model are estimated on daily returns.

The estimated coefficients show significant leverage effect and volatility persistence. For example, volatility persistence in the DCS model is measured by $\beta + \alpha\gamma^2 = 0.9879$. The above empirical regularities are in line with previous studies (see Christoffersen et al. (2014) and Christoffersen et al. (2006) for example).

Table 2 provides supportive evidence for different dynamics of conditional skewness and variance. The coefficients in the dynamic equation of s_t are all significant, and this underscores the necessity and reasonability of incorporating inverse Gaussian innovation $y_{1,t+1}$ in the return process, because the dynamics of the conditional moments s_t has additional information content beyond the conditional variance for specifying the dynamics of the conditional skewness. Moreover, for the DCS, the IG-ARV, and the IG GARCH model, the estimates of η are all negative, and this is consistent with the summary statistics showing that historical returns are left skewed.

5 Option Valuation

In this section, we use the return process defined in Section 2 to derive option valuation formula, using the conditional moment generating function. We present results for the DCS model, as the IG-ARV model can be obtained as a special case.

5.1 Moment Generating Function

To derive option prices in closed form and avoid the need to resort to simulation techniques, a sufficient condition is for the option pricing framework to be affine (Duffie et al. (2000)). In discrete-time, it is sufficient to show that the joint one-step-ahead conditional characteristic function is exponentially linear (Darolles et al. (2006)). In order to obtain the characteristic function of the process,

Table 2: Estimation on Historical Returns and Realized Measures

Estimation on Historical Returns and Realized Measures

Parameters	DCS	IG-ARV	IG GARCH	ARV	HNG
v		796.2165	1047.7570		
		(104.9118)	(24.6388)		
λ_z	1.6800			0.7330	1.49E-06
	(0.0396)			(0.0146)	(0.0040)
λ_y	25.1965				
	(0.0037)				
a		2.35E+04	5.30E+06		
		(262.9164)	(7.15E+05)		
α	4.68E-06			4.82E-06	4.47E-06
	(4.54E-08)			(2.40E-08)	(4.72E-09)
b	-0.9791	-0.1964	-10.7152		
	(0.0041)	(0.0285)	(0.9741)		
β	3.87E-06			3.96E-06	0.7718
	(4.93E-08)			(1.66E-07)	(0.0022)
c	0.0023	1.99E-06	6.25E-06		
	(0.0010)	(1.38E-08)	(2.44E-07)		
γ	459.2242			454.2649	211.3512
	(2.4371)			(1.2055)	(0.8895)
d	1.4667	1.1363			
	(0.0973)	(0.0751)			
σ	9.05E-06			9.15E-06	
	(6.03E-08)			(1.43E-07)	
η	-0.0774	-0.0013	-9.54E-04		
	(0.0387)	(5.93E-05)	(2.24E-05)		
$\pi^{\mathbb{P}}$	0.9879	0.9602	0.9705	0.9948	0.9715
$\mathcal{L}$	59,145	67,428	16,447	57,616	16,384

Notes: Table 2 reports estimation results for the five models using quasi maximum likelihood estimation. For each estimation, we report the coefficients, and the corresponding standard errors are presented in parentheses. To allow for a direct comparison, we also include log likelihoods, $\mathcal{L}$, and volatility persistence, $\pi^{\mathbb{P}}$. Parameter w in the DCS model and parameter ω in all of the five models are directly computed using sample variance and skewness, and thus omitted.

we follow previous studies on closed-form option pricing formula (see, for example, Christoffersen et al. (2006) and Christoffersen et al. (2014)) and derive the moment generating function (MGF).

To begin with, the one-step-ahead MGF under $\mathbb{P}$ measure can be written as

$$\mathbb{E}_t\left[\exp\left(\nu_1 R_{t+1} + \nu_2 h_{t+1} + \nu_3 s_{t+1}\right)\right] = \exp\left(A_1(\nu_1,\nu_2,\nu_3)h_t + A_2(\nu_1,\nu_2,\nu_3)s_t + B(\nu_1,\nu_2,\nu_3)\right) \quad (56)$$

where

$$\begin{aligned}
A_1(\nu_1,\nu_2,\nu_3) &= \nu_1\left(\lambda_z - \frac{1}{2}\right) + \nu_2\beta + m_3 + \frac{m_2^2}{2\left(1-2m_1\right)},\\
A_2(\nu_1,\nu_2,\nu_3) &= \nu_1\left(\lambda_y - \xi\right) + \nu_3 b + 2 - \sqrt{1-2\nu_1\eta_1} - \sqrt{1-2\nu_3 c},\\
B(\nu_1,\nu_2,\nu_3) &= \nu_1 r + \nu_2\omega + \nu_3 w - \frac{1}{2}\log\left(1-2\nu_2\alpha\left(1-\rho^2\right)\right) - \frac{1}{2}\log\left(1-2m_1\right)
\end{aligned}$$

are given by ν_1, ν_2, ν_3, and parameters of the DCS model.

Now we are ready to derive the multi-period moment generating function, $\Psi(\cdot)$. By applying the law of conditional expectation iteration, we have:

$$\begin{aligned}
\Psi_{t,t+M}(u) \equiv \mathbb{E}_t\left[\exp\left(u\sum_{j=1}^{M+1} R_{t+j}\right)\right] &= \mathbb{E}_t\left[\mathbb{E}_{t+1}\left[\exp\left(u\sum_{j=1}^{M+1} R_{t+j}\right)\right]\right]\\
&= \exp\begin{pmatrix} A_1(u, C_1(u,M), C_2(u,M))h_t \\ +A_2(u, C_1(u,M), C_2(u,M))s_t \\ +B(u, C_1(u,M), C_2(u,M)) + D(u,M) \end{pmatrix}.
\end{aligned} \quad (57)$$

The recursive rule can be written as

$$\begin{aligned}
C_1(u, M+1) &= A_1(u, C_1(u,M), C_2(u,M)),\\
C_2(u, M+1) &= A_2(u, C_1(u,M), C_2(u,M)),\\
D(u, M+1) &= B(u, C_1(u,M), C_2(u,M)) + D(u,M),
\end{aligned} \quad (58)$$

where

$$\begin{aligned}
C_1(u,1) &= A_1(u,0,0),\\
C_2(u,1) &= A_2(u,0,0),\\
D(u,1) &= B(u,0,0).
\end{aligned} \quad (59)$$

Proof: See Appendix B. ■

5.2 Risk Neutralization

To derive the option valuation formula, we need to obtain the dynamics under the risk neutral measure. We follow the risk-neutralization method of Christoffersen et al. (2010). The DCS model has four random shocks, $z_{1,t+1}$, $z_{2,t+1}$, $y_{1,t+1}$, and $y_{2,t+1}$. Therefore, we apply the following pricing kernel corresponding to the above four random shocks to derive the dynamics under $\mathbb{Q}$ measure:

$$Z_{t+1} = \frac{\exp\left(\nu_{1,t}z_{1,t+1} + \nu_{2,t}z_{2,t+1} + \nu_{3,t}y_{1,t+1} + \nu_{4,t}y_{2,t+1}\right)}{\mathbb{E}_t\left[\exp\left(\nu_{1,t}z_{1,t+1} + \nu_{2,t}z_{2,t+1} + \nu_{3,t}y_{1,t+1} + \nu_{4,t}y_{2,t+1}\right)\right]}. \tag{60}$$

This risk-neutralization specification is a general setting in option valuation models, see, for example, Corsi et al. (2013), Christoffersen et al. (2014), Majewski et al. (2015), Huang et al. (2017), and Liang et al. (2023).

The no-arbitrage condition, namely that the expectation of returns under $\mathbb{Q}$ measure equals to the risk-free return r, yields

$$\mathbb{E}_t^{\mathbb{Q}}\left[\exp\left(R_{t+1}\right)\right] = \exp(r). \tag{61}$$

The pricing kernel Z_{t+1} builds the relationship between $\mathbb{P}$ measure and $\mathbb{Q}$ measure,

$$\mathbb{E}_t^{\mathbb{Q}}\left[\exp\left(R_{t+1}\right)\right] = \mathbb{E}_t\left[Z_{t+1}\exp\left(R_{t+1}\right)\right], \tag{62}$$

and then we have

$$\mathbb{E}_t\left[Z_{t+1}\exp\left(R_{t+1}\right)\right] = \exp(r). \tag{63}$$

The equivalent condition of the no-arbitrage condition can be derived by equation (63). Similarly, the moment generating function under $\mathbb{Q}$ measure, $\Psi_{t,t+M}^{\mathbb{Q}}(u)$, is obtained using the physical MGF in equation (57) and the mapping relationship determined by the pricing kernel Z_{t+1}.

Now we are ready to obtain the dynamic conditional skewness model under $\mathbb{Q}$ measure. Similar to the DCS model under $\mathbb{P}$ measure, the model under $\mathbb{Q}$ measure also consists of return equation (1*), dynamic equations (2* and 3*), and measurement equations (4* and 5*).

$$R_{t+1} = r - \frac{1}{2}h_t - \xi^* s_t^* + \sqrt{h_t}z_{1,t+1}^* + \eta_1^* y_{1,t+1}^*, \tag{1*}$$

$$h_{t+1} = \omega + \beta h_t + \alpha\left(z_{2,t+1}^* - \gamma^*\sqrt{h_t}\right)^2, \tag{2*}$$

$$s_{t+1}^* = w^* + bs_t^* + c^* y_{2,t+1}^*, \tag{3*}$$

$$\widetilde{\mathrm{RV}}_{t+1} = h_t^* + \sigma\left[\left(z_{2,t+1}^* - \gamma^*\sqrt{h_t}\right)^2 - \left(1 + \gamma^{*2}h_t^{*2}\right)\right], \tag{4*}$$

$$\widetilde{\mathrm{RS}}_{t+1}^* = s_t^* + d^*\left(y_{2,t+1}^* - s_t^*\right). \tag{5*}$$

The above risk neutralization process is detailed in Appendix C.

Proof: See Appendix C. ■

5.3 Option Valuation Formula

At time t, the price of a European call option is given by

$$C\left(t,M\right) = S_t P_1\left(t,M\right) - \exp\left(-rM\right) K P_2\left(t,M\right), \tag{64}$$

where S_t is the price of the underlying asset at time t, K is the strike price, and M denotes maturity. The risk-neutral probabilities $P_1\left(t,M\right)$ and $P_2\left(t,M\right)$ can be computed using Fourier inversion of the risk-neutral conditional characteristic function as follows:

$$\begin{aligned} P_1\left(t,M\right) &= \frac{1}{2} + \int_0^{+\infty} \Re\left[\frac{\Psi_{t,t+M}^{\mathbb{Q}}\left(1+iu\right)\exp\left(-rM - iu\log\left(\frac{K}{S_t}\right)\right)}{\pi i u}\right] du, \\ P_2\left(t,M\right) &= \frac{1}{2} + \int_0^{+\infty} \Re\left[\frac{\Psi_{t,t+M}^{\mathbb{Q}}\left(iu\right)\exp\left(-iu\log\left(\frac{K}{S_t}\right)\right)}{\pi i u}\right] du. \end{aligned} \tag{65}$$

The risk-neutral characteristic function is obtained using the risk-neutral MGF. The price of the corresponding put option can be computed from put-call parity.

6 Option Pricing Performance

To examine whether skewness dynamics and realized measures improve option-pricing accuracy, in this section, we compare the option pricing performance of the new proposed models with nested benchmarks. We first describe the option dataset, and then estimate models to obtain coefficients that are used to conduct out-of-sample evaluations. Finally, we compare out-of-sample performance across models.

6.1 Option Data

We use daily prices of European options on the S&P 500 index. The option data are obtained from OptionMetrics and the VIX data are from Cboe. The sample period is from January 6, 2016 to

December 18, 2019. Following Christoffersen et al. (2006) and Christoffersen et al. (2014), we use call options with maturities of 7-180 days, and compute the mid price of bid and ask quotes on each Wednesday. Among them, prices not satisfying the no-arbitrage condition

$$C(t, M) \geqslant \max(0, S_t - K),$$

or less than 0.375 dollars are excluded. The above process ultimately yields a sample of 173,158 observations.

Table 3 reports summary statistics, and the option data are sorted by moneyness (S/K) and days-to-maturity (DTM). In each category, we report the average option price, the average bid-ask spread, and the number of contracts. Notably, 41.18% of contracts will expire within 30 days, underscoring the importance of studying options with short maturities. As DTM increases, the number of contracts decreases, while the average option price increases. This pattern is align with existing studies such as Christoffersen et al. (2014) and Feunou and Okou (2019).

The dataset includes two subsamples. Data from January 6, 2016 to December 26, 2018 (in-sample) are used to estimate models and obtain coefficients, while data from January 2, 2019 to December 18, 2019 are used to test out-of-sample option pricing performance. We show the implied volatility (IV) curve for in-sample and out-of-sample options in Figure 6. Figure 6 contains four panels: Panels (a) and (b) are the IV curves for in-sample options with maturities shorter than or at least 30 days, respectively; while Panels (c) and (d) show the corresponding IV curves for out-of-sample options.

Table 3: Summary Statistics of S&P 500 Index Option Data

		OTM		ATM		ITM		Subtotal
		S/K<0.94	0.94⩽S/K<0.97	0.97⩽S/K<1	1⩽S/K<1.03	1.03⩽S/K<1.06	1.06⩽S/K	
DTM<30	Price	1.0140	2.5001	10.9120	48.0328	107.2964	234.9214	34.6327
	Bid-Ask Spread	0.2583	0.2583	0.4000	1.2301	3.2344	5.3573	0.9928
	Number	2,175	11,357	29,137	20,769	5,679	2,188	71,305
30⩽DTM<60	Price	1.8322	5.5174	22.6246	63.5765	118.3561	258.9795	41.5437
	Bid-Ask Spread	0.3002	0.3368	0.5657	1.0227	1.9713	3.9288	0.8209
	Number	8,062	16,468	19,311	12,672	4,773	2,911	64,197
60⩽DTM<90	Price	3.9381	12.7058	38.4705	80.0355	135.3762	291.7120	55.8299
	Bid-Ask Spread	0.3923	0.5117	0.7622	1.1039	1.5388	3.3761	0.8209
	Number	3,873	4,779	5115	3317	1482	1262	19,828
90⩽DTM<120	Price	5.6319	20.1375	53.4278	94.5147	149.4875	341.1983	67.0211
	Bid-Ask Spread	0.4572	0.6459	0.9278	1.2554	1.7240	3.4247	1.0270
	Number	2,478	2290	2379	1396	566	754	9863
120⩽DTM<150	Price	7.1442	29.8769	66.0420	109.6244	160.9370	354.8294	77.8500
	Bid-Ask Spread	0.5092	0.7677	1.0203	1.2652	1.9026	3.5783	1.1274
	Number	1,622	970	962	583	274	474	4,885
150⩽DTM	Price	10.2967	40.1327	76.0613	120.4613	171.8856	367.7687	86.8600
	Bid-Ask Spread	0.6382	0.9850	1.1877	1.4881	2.0535	3.5153	1.2807
	Number	1,122	581	553	320	170	334	3080
Subtotal	Price	3.5860	7.6388	20.6123	58.9689	118.4182	275.6942	43.6152
	Bid-Ask Spread	0.3712	0.3765	0.5278	1.1556	2.4648	4.1489	0.9306
	Number	19,332	36,445	57,457	39,057	12,944	7,923	173,158

Notes: Table 3 reports the summary statistics of the S&P 500 index option data sorted by moneyness and maturity. For each category, we report average option price, average bid-ask spread, and the number of contracts. The sample covers the period from January 6, 2016 to December 18, 2019, and we use data on Wednesdays. In this table, S represents the price of S&P 500 index, and K is the strike price. "OTM", "ATM", and "ITM" denotes out-of-the-money, at-the-money, and in-the-money options, respectively.

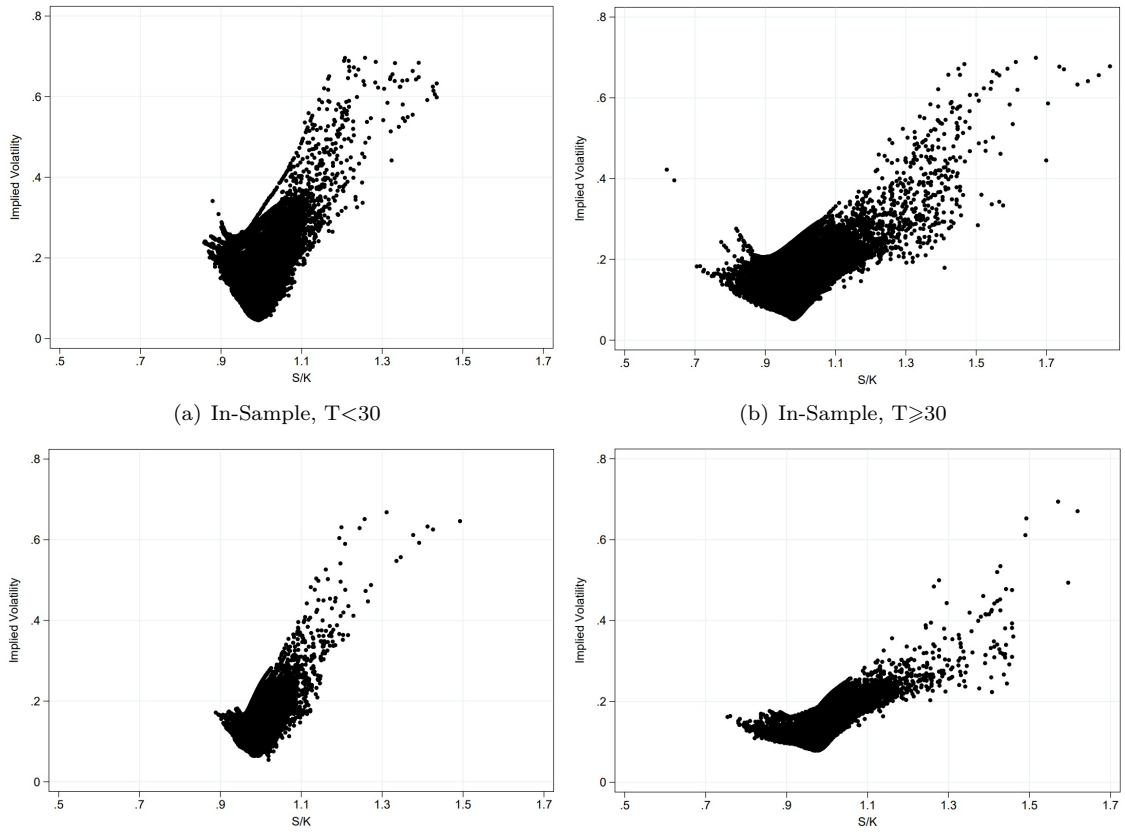

(a) In-Sample, T<30

(b) In-Sample, T⩾30

(c) Out-of-Sample, T<30

(d) Out-of-Sample, T⩾30

Figure 6: Implied Volatility Curves

Notes: Figure 6 shows the implied volatility patterns of the S&P 500 index options with short and long maturities. Specifically, Panel (a) is the IV curve for in-sample options with maturities less than 30 days, covering 49,391 contracts; Panel (b) plots the IV curve for in-sample options with maturities of at least 30 days, with a total of 71,896 option contracts; Panels (c) and (d) show the IV curves for out-of-sample options with maturities below and above 30 days, and the number of corresponding contracts are 21,914 and 29,957, respectively.

Figure 6 shows that options with short maturities exhibit a more pronounced volatility smirk. This finding is in line with Christoffersen et al. (2006), and it is robust in both in-sample and out-of-sample periods, suggesting the importance of the deviations between market prices and theoretical prices from the Black–Scholes formula for options with short maturities. Besides, Table 4 provides additional evidence supporting the more significant volatility smirk for options with

short maturities. We report the average implied volatility of different moneyness and maturity combinations, and the partition criteria are the same as Table 3. We find that, for both in-sample and out-of-sample periods, the implied volatility difference between deep ITM and OTM calls are larger for short-term options ($T < 30$) than for options with long maturities ($T \geqslant 150$).

Table 4: Implied Volatility, In-Sample and Out-of-Sample

	Days-to-Maturity					
Moneyness	T<30	30⩽T<60	60⩽T<90	90⩽T<120	120⩽T<150	T⩾150
Panel A. In-Sample						
S/K<0.94	0.1753	0.1337	0.1204	0.1106	0.1084	0.1116
	(1,801)	(5,880)	(2,640)	(1,622)	(1,052)	(716)
0.94⩽S/K<0.97	0.1259	0.1004	0.1018	0.1044	0.1085	0.1169
	(7,432)	(11,402)	(3,295)	(1,490)	(593)	(350)
0.97⩽S/K<1	0.1005	0.1020	0.1117	0.1201	0.1227	0.1275
	(20,011)	(13,775)	(3,610)	(1,544)	(575)	(350)
1⩽S/K<1.03	0.1233	0.1236	0.1314	0.1383	0.1394	0.1441
	(14,472)	(9,180)	(2,440)	(921)	(337)	(206)
1.03⩽S/K<1.06	0.1717	0.1511	0.1498	0.1555	0.1545	0.1599
	(4,105)	(3,753)	(1,099)	(385)	(185)	(118)
1.06⩽S/K	0.2877	0.2172	0.2058	0.2113	0.2033	0.2008
	(1,570)	(2,327)	(962)	(542)	(324)	(223)
Panel B. Out-of-Sample						
S/K<0.94	0.1377	0.1199	0.1164	0.1138	0.1156	0.1174
	(374)	(2,182)	(1,233)	(856)	(570)	(406)
0.94⩽S/K<0.97	0.1146	0.1134	0.1134	0.1180	0.1235	0.1263
	(3,925)	(5,066)	(1,484)	(800)	(377)	(231)
0.97⩽S/K<1	0.1147	0.1210	0.1292	0.1355	0.1406	0.1439
	(9,126)	(5,536)	(1,505)	(835)	(387)	(203)
1⩽S/K<1.03	0.1437	0.1455	0.1488	0.1522	0.1547	0.1597
	(6,297)	(3,492)	(877)	(475)	(246)	(114)
1.03⩽S/K<1.06	0.1808	0.1725	0.1694	0.1732	0.1725	0.1758
	(1,574)	(1,020)	(383)	(181)	(89)	(52)
1.06⩽S/K	0.2592	0.2230	0.2189	0.2222	0.2199	0.2148
	(618)	(584)	(300)	(212)	(150)	(111)

Notes: Table 4 reports the average implied volatility of the S&P 500 index options in different moneyness and maturity combinations. Moneyness is measured by S/K, where S is the close price of the S&P 500 index and K is the strike price of the S&P 500 index option. The number of contracts in each combination is reported in parentheses. The in-sample period ranges from January 6, 2016 to December 26, 2018, and the out-of-sample period covers from January 2, 2019 to December 18, 2019.

6.2 Joint Estimation

We follow recent studies (see Christoffersen et al. (2014), Christoffersen et al. (2015), and Feunou and Okou (2019), among others) and use the vega-weighted root-mean-squared error (VWRMSE) for optimization on options:

$$\text{VWRMSE} \equiv \sqrt{\frac{1}{N}\sum_{j=1}^{N} e_j^2} \equiv \sqrt{\frac{1}{N}\sum_{j=1}^{N}\left(\frac{C_j^{\text{MKT}} - C_j^{\text{MOD}}}{\text{BSV}_j^{\text{MKT}}}\right)^2}, \tag{66}$$

where C_j^{MOD} denotes the model-based price of option j, C_j^{MKT} is the market price, and $\text{BSV}_j^{\text{MKT}}$ represents the Black-Scholes vega, the derivative with respect to volatility, computed using the market implied volatility. According to Trolle and Schwartz (2009), this scaling method simplifies the log likelihood function. Specifically, the log likelihood function based on Gaussian vega-weighted option errors is given by

$$\mathcal{L}^O \propto -\frac{1}{2}\sum_{j=1}^{N}\left\{\ln\left(\text{VWRMSE}^2\right) + \frac{e_j^2}{\text{VWRMSE}^2}\right\}. \tag{67}$$

Now we are ready to estimate the model with the joint log likelihood function of the observed variables and pricing errors. We optimize the joint log likelihood function that contains two parts: quasi log likelihoods of returns and realized components ($\mathcal{L}^{\mathbb{P}}$ in Equation (55)) and option-based log likelihoods ($\mathcal{L}^O$ in Equation (67)),

$$\mathcal{L} = \mathcal{L}^{\mathbb{P}} + \mathcal{L}^O. \tag{68}$$

The estimation results are reported in Table 5, and we find similar evidence with those in Table 2, supporting different evolution of conditional variance and skewness. Again, the coefficients in the dynamic equation of s_t are all significant. In addition, the estimates of η are still negative, and this is consistent with coefficients in Table 2 as well as the summary statistics, showing that historical returns are left skewed.

6.3 Pricing Performance Evaluation

To compare the option pricing accuracy across different models, we use the implied volatility root mean squared error (IVRMSE), which measures the difference between model-based and market implied volatilities. We refer to Renault (1997) for a detailed discussion on the benefits of using the IVRMSE for evaluating option-pricing performance.

Table 5: In-Sample Joint Estimation Results

In-Sample Joint Estimation Results

Parameters	DCS	IG-ARV	IG GARCH	ARV	HNG
v		1.59E+03	1.44E+03		
		(16.9307)	(79.5929)		
λ_z	5.3870			0.5696	10.1137
	(0.1195)			(0.8636)	(0.1417)
λ_y	38.0566				
	(3.03E-05)				
a		5.13E+05	2.29E+04		
		(1.47E+05)	(28.4641)		
α	2.31E-06			5.90E-06	1.28E-08
	(9.40E-08)			(1.39E-06)	(1.89E-07)
b	-0.7927	-0.7682	0.9377		
	(0.0013)	(0.0299)	(0.0080)		
β	0.1587			0.0047	0.9866
	(0.0709)			(0.1110)	(0.0117)
c	1.82E-06	5.56E-07	3.62E-08		
	(1.44E-07)	(1.70E-08)	(7.47E-09)		
γ	590.5071			95.2821	94.4087
	(31.8310)			(1.0004)	(0.2034)
d	0.6597	5.7028			
	(0.0003)	(0.1972)			
σ	4.04E-06			1.66E-05	
	(2.48E-07)			(1.90E-06)	
ρ	0.2675			0.3966	
	(0.0277)			(0.0450)	
η	-3.90E-05	-0.0006	-0.0014		
	(7.98E-05)	(1.27E-06)	(0.0001)		
γ^*	420.0018			393.6478	
	(0.7229)			(44.7177)	
ν_3	0.4992				
	(9.97E-05)				
$\pi^{\mathbb{Q}}$	0.9891	0.9690	0.9999	0.9190	0.9867
$\mathcal{L}$	423,378	172,181	149,528	149,294	85,584

Notes: Table 5 reports the joint estimation results for the DCS model, the IG-ARV model, and nested benchmarks. For each model, we report the estimated coefficients, and their corresponding standard errors are in parentheses. We also report the log likelihood, $\mathcal{L}$, and the volatility persistence under $\mathbb{Q}$ measure, $\pi^{\mathbb{Q}}$. Parameters w and ω are directly computed using sample variance and skewness, and thus omitted. The in-sample period spans from January 6, 2016 to December 26, 2018.

To compute the IVRMSE, we first obtain the model-based implied volatility, $\mathrm{IV}_j^{\mathrm{Mod}}$, by using the model-based option prices and inverting the Black-Scholes (BS) formula (Black and Scholes (1973)):

$$\mathrm{IV}_j^{\mathrm{Mod}} = \mathrm{BS}^{-1}\left(C_j^{\mathrm{Mod}}\right). \tag{69}$$

Similarly, the market implied volatility, $\mathrm{IV}_j^{\mathrm{Mkt}}$, is derived from:

$$\mathrm{IV}_j^{\mathrm{Mkt}} = \mathrm{BS}^{-1}\left(C_j^{\mathrm{Mkt}}\right). \tag{70}$$

The implied volatility error, e_{j}, measures the difference between the above two implied volatilities:

$$e_j = \mathrm{IV}_j^{\mathrm{Mkt}} - \mathrm{IV}_j^{\mathrm{Mod}}. \tag{71}$$

The IVRMSE is then calculated as:

$$\mathrm{IVRMSE} = \sqrt{\frac{1}{N}\sum_{j=1}^{N} e_j^2}, \tag{72}$$

where N denotes the total number of options in the sample. The IVRMSE effectively quantifies the overall deviation between model and market implied volatilities, facilitating a consistent evaluation of option valuation efficacy.

6.4 In-Sample Pricing Performance

We first compare the in-sample option pricing accuracy using model coefficients from Table 5, the corresponding IVRMSEs are reported in Table 6. The option contracts are sorted by moneyness, maturity, and the Cboe VIX level. The categories for moneyness and maturity are the same as in Table 3. The VIX data come from the Cboe website.[5] Within our option sample, the VIX level varies from 9.15 to 30.41.

Overall, the DCS model performs best among the five models, followed by the IG-ARV model. This result provides direct evidence of the advance in option pricing accuracy brought by the flexibility that the model offers for skewness dynamics and timely arrived information from the new constructed realized components. Among the benchmark models, the ARV model obtains the smallest option pricing error, and the DCS model achieves a 5.25% reduction in IVRMSE relative to

[5] https://www.cboe.com/tradable_products/vix/vix_historical_data/

Table 6: In-Sample IVRMSE by Moneyness, Maturity, and VIX

In-Sample IVRMSE by Moneyness, Maturity, and VIX

Model	Total	S/K<0.94	0.94⩽S/K<0.97	0.97⩽S/K<1.00	1.00⩽S/K<1.03	1.03⩽S/K<1.06	S/K⩾1.06
Panel A. Partitioned by Moneyness							
DCS	**4.9196**	6.2735	5.0014	**4.5000**	4.2829	**4.9928**	**6.1880**
IG-ARV	5.0491	3.6138	**4.0195**	4.6892	4.1139	5.0306	12.4631
IG GARCH	5.5214	4.1457	4.7737	4.7458	5.8600	7.7241	8.9867
ARV	5.1926	**3.5628**	4.0493	4.6204	**4.0885**	5.3019	13.6264
HNG	6.6547	6.0758	5.0971	4.9979	6.7561	9.6992	13.3523
Model	Total	T<30	30⩽T<60	60⩽T<90	90⩽T<120	120⩽T<150	T⩾150
Panel B. Partitioned by Maturity							
DCS	**4.9196**	**5.4283**	**4.2397**	**3.4255**	**3.2412**	**3.0502**	**3.2105**
IG-ARV	5.0491	5.7722	4.6554	4.2348	4.1362	3.9626	3.9753
IG GARCH	5.5214	5.9318	5.1291	5.3340	5.4201	5.3090	5.7084
ARV	5.1926	5.9431	4.7960	4.3444	4.1903	4.0167	4.0035
HNG	6.6547	8.3071	5.5838	4.6357	4.4820	4.1400	4.1123
Model	Total	VIX<12	12⩽VIX<15	15⩽VIX<18	18⩽VIX<21	21⩽VIX<24	VIX⩽24
Panel C. Partitioned by VIX Level							
DCS	**4.9196**	4.5700	3.9517	4.1164	5.3474	6.3942	**8.5255**
IG-ARV	5.0491	4.9584	4.0235	**3.8429**	**5.1712**	**5.9086**	9.0867
IG GARCH	5.5214	**2.5901**	**3.7295**	5.4841	8.0841	9.1287	11.6042
ARV	5.1926	4.9696	4.1692	4.2375	5.4880	6.1936	9.2166
HNG	6.6547	3.8452	4.8011	6.3850	9.3744	10.2843	13.6284

Notes: Table 6 reports the IVRMSEs to compare the in-sample option-pricing performance across models. The IVRMSEs are sorted by moneyness, maturity, and the Cboe VIX level. Panel A reports the IVRMSEs for contracts sorted by moneyness (measured by S/K). Panel B presents the IVRMSEs sorted by days to maturity (T). Panel C shows the IVRMSEs sorted by the VIX level on quotation day. For each category, the IVRMSEs are expressed in percentages, with the smallest value marked in bold. The in-sample period spans from January 6, 2016 to December 26, 2018.

the ARV model. Models that rely on daily returns rather than realized measures to update dynamics of variance and skewness, the IG GARCH and the HNG, result in larger IVRMSEs, and this finding is in line with existing studies (see Christoffersen et al. (2014), Feunou and Okou (2019), and Liang et al. (2023), among others). Moreover, considering asymmetry in returns improves option pricing accuracy, as evidenced by a 17.03% reduction in IVRMSE by the IG GARCH model relative to the HNG model.

Panel A shows the superior performance of the DCS model in pricing deep in-the-money call options, especially when S/K$\geqslant$1.06. Compared to models not allowing for dynamic skewness in returns, i.e., the ARV and the HNG, the DCS model achieves an improvement of 54.58% and 53.65% in option pricing accuracy, respectively. This result emphasizes the importance of effectively modeling skewness to capture the volatility smirk. The above finding is consistent with previous studies such as Christoffersen et al. (2006) and Feunou and Tédongap (2012).

As is evident in Panel B, the overall improvement achieved by the DCS model is not driven by any specific range of maturity. Importantly, it is noteworthy that the DCS model demonstrates particularly strong performance when pricing options with maturity less than 30 days. This subset of contracts, as shown in Table 3, constitutes 41.17% of our sample. Moreover, from Figure 6 and Table 4, options with short maturities exhibit a more pronounced volatility smirk, suggesting the importance of the deviations between market prices and theoretical prices from the Black–Scholes formula for options with short maturities. Results in Panel B show that, the DCS model gains an even larger improvement in pricing short-term options.

From Panel C, the DCS model performs best during highly volatile periods when all models obtain maximum pricing errors. The IG-ARV model emerges as the closest competitor. Considering different dynamic processes of conditional variance and skewness, as well as constructing realized components to update the dynamics reduces pricing error by 26.53%, compared to the IG GARCH model.

6.5 Out-of-Sample Pricing Performance

To provide more convincing evidence, we compare out-of-sample option-pricing performance, and the results are reported in Table 7. In out-of-sample tests, we obtain consistent findings. Once again, the DCS model performs best among the five models, and the IG-ARV model maintains the second place. The DCS model achieves an out-of-sample gain of 12.25% compared to the second

best model.

From Panel A, the DCS model performs best for the ATM and ITM calls. In particular, for the deep ITM calls (S/K$\geqslant$1.06), the DCS model achieves an even larger out-of-sample gain of 50.35%, compared to the second best. Panel B shows that the DCS model performs best for options with short maturities (T<30), with an improvement of 51.82% relative to the second best. We can see clearly in Panel C that the pricing errors of all models increase in highly volatile times, however, the DCS model still maintains superior performance and achieves a larger improvement of 20.63% when VIX$\geqslant$21. Therefore, we conclude here that the DCS model has even better performance in pricing deep in-the-money calls, options with shorter maturities, and during highly volatile periods.

7 Conclusion

This paper proposes and tests a discrete-time affine option-pricing model with dynamic conditional skewness in returns. We refer to this model as the Dynamic Conditional Skewness model. The DCS model features different dynamics for conditional skewness and variance. To stress the difference in information, we use alternative realized measures constructed from high-frequency historical returns to update skewness and variance dynamics.

From a theoretical viewpoint, the affine structure of the new option pricing framework enables us to derive analytical valuation formulas nesting popular specifications. Analytical formulas explicitly quantify the impact of model parameters on critical conditional moments, facilitate the estimation procedure, allow for a direct comparison of nested models, and avoids the need to resort to simulation techniques.

Empirically, the flexibility that the model offers for conditional skewness as well as high-frequency information from the underlying asset contribute to superior performance upon benchmark models using S&P 500 index options. Overall, the joint modeling of dynamic conditional skewness and realized measures leads to an out-of-sample gain of 12.25% in pricing accuracy. The improvements are more pronounced for deep in-the-money calls, options with shorter maturities, and during highly volatile periods.

The DCS framework can be extended in a number of ways. For instance, it is important to consider jump variation in conditional skewness dynamics. Although the leverage effect produces negative skewness during periods of low sampling frequency (e.g., monthly or quarterly), during

Table 7: Out-of-Sample IVRMSE by Moneyness, Maturity, and VIX

Out-of-Sample IVRMSE by Moneyness, Maturity, and VIX

Model	Total	S/K<0.94	0.94⩽S/K<0.97	0.97⩽S/K<1.00	1.00⩽S/K<1.03	1.03⩽S/K<1.06	S/K⩾1.06
Panel A. Partitioned by Moneyness							
DCS	**3.7494**	4.5350	2.9774	3.4186	**4.1685**	**4.4916**	**4.2970**
IG-ARV	4.2731	2.0634	2.1031	**2.9755**	4.5812	7.0287	12.6571
IG GARCH	4.6306	2.9356	3.4168	4.1771	5.0972	7.2563	8.6555
ARV	4.5047	**2.0113**	**2.0900**	3.0136	4.8120	7.4324	13.8095
HNG	4.7178	5.1024	3.2808	3.4137	4.8621	6.7701	11.3988
Model	Total	T<30	30⩽T<60	60⩽T<90	90⩽T<120	120⩽T<150	T⩾150
Panel B. Partitioned by Maturity							
DCS	**3.7494**	**2.2225**	4.3062	4.5118	4.9840	5.3646	5.6534
IG-ARV	4.2731	4.6134	**3.8304**	**4.0821**	4.2517	4.5032	4.6807
IG GARCH	4.6306	5.2082	4.2221	4.1291	**3.9324**	**3.9267**	**4.2980**
ARV	4.5047	4.9332	4.0074	4.2338	4.3888	4.5992	4.7648
HNG	4.7178	4.8858	4.4087	4.6811	4.8880	5.0694	5.1976
Model	Total	VIX<12	12⩽VIX<15	15⩽VIX<18	18⩽VIX<21	21⩽VIX<24	
Panel C. Partitioned by VIX Level							
DCS	**3.7494**	2.8379	**3.0237**	3.7135	**4.7120**	**5.9779**	
IG-ARV	4.2731	2.9249	3.2738	3.7635	5.8427	7.7271	
IG GARCH	4.6306	4.5490	3.8357	**3.3302**	6.1791	9.0525	
ARV	4.5047	2.9647	3.5161	4.0586	6.0852	7.8533	
HNG	4.7178	**2.6555**	3.5909	4.5484	6.4670	7.5326	

Notes: Table 7 reports the IVRMSEs to compare the out-of-sample option-pricing performance across models. The IVRMSEs are sorted by moneyness, maturity, and the Cboe VIX level. Panel A reports the IVRMSEs for contracts sorted by moneyness (measured by S/K). Panel B presents the IVRMSEs sorted by days to maturity (T). Panel C shows the IVRMSEs sorted by the VIX level on quotation day. For each category, the IVRMSEs are expressed in percentages, with the smallest value marked in bold. The out-of-sample period spans from January 2, 2019 to December 18, 2019.

intraday periods the instantaneous leverage effect is very weak. Feunou et al. (2016) have observed that in data sampled within a trading day, conditional skewness is driven purely by jumps. In addition, Feunou and Okou (2019) use signed jump variation, capturing the difference between positive and negative jump possibilities, as a measure of realized skewness. Another interesting extension is to study the role of conditional kurtosis in modeling underlying asset returns and pricing derivatives.

References

D. Amaya, P. Christoffersen, K. Jacobs, and A. Vasquez. Does realized skewness predict the cross-section of equity returns? *Journal of Financial Economics*, 118(1):135–167, 2015.

T. G. Andersen, T. Bollerslev, F. X. Diebold, and H. Ebens. The distribution of realized stock return volatility. *Journal of financial economics*, 61(1):43–76, 2001a.

T. G. Andersen, T. Bollerslev, F. X. Diebold, and P. Labys. The distribution of realized exchange rate volatility. *Journal of the American statistical association*, 96(453):42–55, 2001b.

T. G. Andersen, T. Bollerslev, F. X. Diebold, and P. Labys. Modeling and forecasting realized volatility. *Econometrica*, 71(2):579–625, 2003.

O. E. Barndorff-Nielsen and N. Shephard. Econometric analysis of realized volatility and its use in estimating stochastic volatility models. *Journal of the Royal Statistical Society Series B: Statistical Methodology*, 64(2):253–280, 2002.

O. E. Barndorff-Nielsen, S. Kinnebrock, and N. Shephard. Measuring downside risk-realised semivariance. *CREATES Research Paper*, (2008-42), 2008.

F. Black and M. Scholes. The pricing of options and corporate liabilities. *Journal of political economy*, 81(3):637–654, 1973.

M. Chernov and E. Ghysels. A study towards a unified approach to the joint estimation of objective and risk neutral measures for the purpose of options valuation. *Journal of financial economics*, 56(3):407–458, 2000.

P. Christoffersen and K. Jacobs. Which garch model for option valuation? *Management science*, 50(9):1204–1221, 2004.

P. Christoffersen, S. Heston, and K. Jacobs. Option valuation with conditional skewness. *Journal of Econometrics*, 131(1-2):253–284, 2006.

P. Christoffersen, R. Elkamhi, B. Feunou, and K. Jacobs. Option valuation with conditional heteroskedasticity and nonnormality. *The Review of Financial Studies*, 23(5):2139–2183, 2010.

P. Christoffersen, B. Feunou, K. Jacobs, and N. Meddahi. The economic value of realized volatility: Using high-frequency returns for option valuation. *Journal of Financial and Quantitative Analysis*, 49(3):663–697, 2014.

P. Christoffersen, B. Feunou, and Y. Jeon. Option valuation with observable volatility and jump dynamics. *Journal of Banking & Finance*, 61:S101–S120, 2015.

F. Corsi, N. Fusari, and D. La Vecchia. Realizing smiles: Options pricing with realized volatility. *Journal of Financial Economics*, 107(2):284–304, 2013.

S. Darolles, C. Gourieroux, and J. Jasiak. Structural laplace transform and compound autoregressive models. *Journal of Time Series Analysis*, 27(4):477–503, 2006.

Z. Ding and C. W. Granger. Modeling volatility persistence of speculative returns: a new approach. *Journal of econometrics*, 73(1):185–215, 1996.

D. Duffie, J. Pan, and K. Singleton. Transform analysis and asset pricing for affine jump-diffusions. *Econometrica*, 68(6):1343–1376, 2000.

B. Feunou and C. Okou. Good volatility, bad volatility, and option pricing. *Journal of financial and quantitative analysis*, 54(2):695–727, 2019.

B. Feunou and R. Tédongap. A stochastic volatility model with conditional skewness. *Journal of Business & economic statistics*, 30(4):576–591, 2012.

B. Feunou, M. R. Jahan-Parvar, and R. Tédongap. Which parametric model for conditional skewness? *The European Journal of Finance*, 22(13):1237–1271, 2016.

L. Forsberg and T. Bollerslev. Bridging the gap between the distribution of realized (ecu) volatility and arch modelling (of the euro): the garch-nig model. *Journal of Applied Econometrics*, 17(5): 535–548, 2002.

S. L. Heston. A closed-form solution for options with stochastic volatility with applications to bond and currency options. *The review of financial studies*, 6(2):327–343, 1993.

S. L. Heston and S. Nandi. A closed-form garch option valuation model. *The review of financial studies*, 13(3):585–625, 2000.

G. X. Hu, J. Pan, J. Wang, and H. Zhu. Premium for heightened uncertainty: Explaining pre-announcement market returns. *Journal of Financial Economics*, 145(3):909–936, 2022.

Z. Huang, T. Wang, and P. R. Hansen. Option pricing with the realized garch model: An analytical approximation approach. *Journal of Futures Markets*, 37(4):328–358, 2017.

M. B. Jensen and A. Lunde. The nig-s&arch model: a fat-tailed, stochastic, and autoregressive conditional heteroskedastic volatility model. *The Econometrics Journal*, 4(2):319–342, 2001.

C. S. Jones. The dynamics of stochastic volatility: evidence from underlying and options markets. *Journal of econometrics*, 116(1-2):181–224, 2003.

F. Liang, L. Du, and Z. Huang. Option pricing with overnight and intraday volatility. *Journal of Futures Markets*, 43(11):1576–1614, 2023.

D. O. Lucca and E. Moench. The pre-fomc announcement drift. *The Journal of finance*, 70(1): 329–371, 2015.

A. A. Majewski, G. Bormetti, and F. Corsi. Smile from the past: A general option pricing framework with multiple volatility and leverage components. *Journal of Econometrics*, 187(2):521–531, 2015.

A. Neuberger. Realized skewness. *The Review of Financial Studies*, 25(11):3423–3455, 2012.

E. Renault. Econometric models of option pricing errors", advances in economics and econometrics: theory and applications, eds d. kreps and k. wallis, vol. iii, 221-278, 1997.

A. B. Trolle and E. S. Schwartz. Unspanned stochastic volatility and the pricing of commodity derivatives. *The Review of Financial Studies*, 22(11):4423–4461, 2009.

A. Wald. *Sequential Analysis*. John Wiley & Sons, New York, 1947.

Appendices

Appendix A Proof of Moment Matching

Based on the return process of the IG-ARV model specified in equation (17), the conditional expectation and variance of R_{t+1} can be derived as

$$\mathbb{E}_t\left[R_{t+1}\right] = r + \left(v + \frac{1}{\eta}\right) h_t^{\mathrm{RV}}, \tag{A-1}$$

$$\mathrm{Var}_t\left[R_{t+1}\right] = h_t^{\mathrm{RV}}. \tag{A-2}$$

In the ARV model, the conditional expectation of R_{t+1} is:

$$\mathbb{E}_t\left[R_{t+1}\right] = r + \lambda h_t^{\mathrm{RV}}. \tag{A-3}$$

Therefore, the following parameterization builds the equivalence of conditional expectation of return in the IG-ARV and the ARV model:

$$v + \frac{1}{\eta} = \lambda. \tag{A-4}$$

Moreover, the equivalence of $\mathbb{E}_t[h_{t+1}^{\mathrm{RV}}]$, $\mathrm{Var}_t[h_{t+1}^{\mathrm{RV}}]$, and $\mathrm{Var}_t\left[\mathrm{RV}_{t+1}\right]$ in the IG-ARV and the ARV model,

$$\mathbb{E}_t[h_{t+1}^{\mathrm{RV}}] = \left(w + a\eta^4\right) + \left(b + \frac{c}{\eta^2} + a\eta^2\right) h_t^{\mathrm{RV}} = (\omega + \alpha) + \left(\beta + \alpha\gamma^2\right) h_t^{\mathrm{RV}}, \tag{A-5}$$

$$\mathrm{Var}_t[h_{t+1}^{\mathrm{RV}}] = \left(\frac{c^2}{\eta^2} - 2ca\eta^2 + a\eta^6\right) h_t^{RV} + 2a^2\eta^8 = 2\alpha^2 + 4\alpha^2\gamma^2 h_t^{\mathrm{RV}}, \tag{A-6}$$

$$\mathrm{Var}_t\left[\mathrm{RV}_{t+1}\right] = 2\sigma^2 + 4\sigma^2\gamma^2 h_t^{\mathrm{RV}} = d^2\left(\left(\frac{c^2}{\eta^2} - 2ca\eta^2 + a\eta^6\right) h_t^{RV} + 2a^2\eta^8\right), \tag{A-7}$$

requires

$$\begin{aligned}
&w + a\eta^4 = \omega + \alpha, \quad b + \frac{c}{\eta^2} + a\eta^2 = \beta + \alpha\gamma^2, \\
&\frac{c^2}{\eta^2} - 2ca\eta^2 + a\eta^6 = 4\alpha^2\gamma^2, \quad a^2\eta^8 = \alpha^2, \\
&\sigma^2 = d^2a^2\eta^8, \quad 4\sigma^2\gamma^2 = d^2\left(\frac{c^2}{\eta^2} - 2ca\eta^2 + a\eta^6\right).
\end{aligned}$$

Appendix B Moment Generating Function

To begin with, consider the one-step-ahead MGF under $\mathbb{P}$ measure,

$$\begin{aligned}
&\mathbb{E}_t\left[\exp\left(\nu_1 R_{t+1}+\nu_2 h_{t+1}+\nu_3 s_{t+1}\right)\right] \\
&=\mathbb{E}_t\left[\exp\left(\begin{array}{c}\nu_1\left(r+\left(\lambda_z-\frac{1}{2}\right)h_t+\left(\lambda_y-\xi\right)s_t+\sqrt{h_t}z_{1,t+1}+\eta_1 y_{1,t+1}\right)\\ +\nu_2\left(\omega+\beta h_t+\alpha\left(z_{2,t+1}-\gamma\sqrt{h_t}\right)^2\right)\\ +\nu_3\left(w+bs_t+cy_{2,t+1}\right)\end{array}\right)\right] \\
&=\exp\left(\nu_1 r+\nu_2\omega+\nu_3 w+\left(\nu_1\left(\lambda_z-\frac{1}{2}\right)+\nu_2\beta\right)h_t+\left(\nu_1\left(\lambda_y-\xi\right)+\nu_3 b\right)s_t\right) \\
&\quad\cdot\underbrace{\mathbb{E}_t\left[\exp\left(\nu_1\sqrt{h_t}z_{1,t+1}+\nu_2\alpha\left(z_{2,t+1}-\gamma\sqrt{h_t}\right)^2\right)\right]}_{\text{(A)}}\cdot\underbrace{\mathbb{E}_t\left[\left(\nu_1\eta_1 y_{1,t+1}\right)\right]}_{\text{(B)}}\cdot\underbrace{\mathbb{E}_t\left[\exp\left(\nu_3 c y_{2,t+1}\right)\right]}_{\text{(C)}}
\end{aligned} \tag{B-1}$$

To derive Terms (A), (B), and (C), we need the following results.

Lemma 1 *Using the Cholesky representation, we can rewrite*

$$z_{1,t+1}=\rho z_{2,t+1}+\sqrt{1-\rho^2}z_{3,t+1},$$

where

$$\begin{pmatrix} z_{2,t+1}\\ z_{3,t+1}\end{pmatrix}\overset{i.i.d}{\sim}\mathcal{N}\left(\begin{pmatrix}0\\0\end{pmatrix},\begin{pmatrix}1&0\\0&1\end{pmatrix}\right).$$

Proof: *The Cholesky decomposition applies to a symmetric, positive definite matrix, denoted as* $\mathbf{X}$*, and is represented as:*

$$\mathbf{L}=\mathrm{Chol}(\mathbf{X})$$

In this representation, $\mathbf{L}$ *is a lower triangular matrix which satisfies the condition* $\mathbf{L}\mathbf{L}^T=\mathbf{X}$*. Consider the Cholesky decomposition of the covariance matrix:*

$$\begin{pmatrix}1&\rho\\ \rho&1\end{pmatrix}=\begin{pmatrix}a&0\\ b&c\end{pmatrix}\begin{pmatrix}a&b\\ 0&c\end{pmatrix},$$

we obtain $a=1,\quad b=\rho,\quad c=\sqrt{1-\rho^2}$. ■

Lemma 2 *For any* $z\overset{i.i.d}{\sim}\mathcal{N}(0,1)$*, we have*

$$\log\mathbb{E}\left[\exp\left(a(z+b)^2\right)\right]=\frac{ab^2}{1-2a}-\frac{1}{2}\log(1-2a).$$

Proof:

$$\begin{aligned}\log \mathbb{E}\left[\exp\left(a(z+b)^2\right)\right] &= \log \int_{-\infty}^{\infty} \frac{1}{\sqrt{2\pi}} \exp\left(az^2 + 2abz + b^2 - \frac{1}{2}z^2\right) dz \\ &= \log \int_{-\infty}^{\infty} \frac{1}{\sqrt{2\pi}} \exp\left(-\frac{1}{2}\left(\sqrt{1-2a}z - \frac{2ab}{\sqrt{1-2a}}\right)^2 + \frac{ab^2}{1-2a}\right) dz \\ &= \frac{ab^2}{1-2a} - \frac{1}{2}\log(1-2a).\end{aligned}$$

■

Lemma 3 *For any* $y \overset{i.i.d}{\sim} IG(\delta)$*, the moment generating function is given by*

$$\mathbb{E}\left[\exp\left(\phi y\right)\right] = \exp\left(\delta - \delta\sqrt{1-2\phi}\right).$$

Proof:

$$\begin{aligned}\mathbb{E}\left[\exp\left(\phi y\right)\right] &= \int_0^{\infty} \exp\left(\phi y\right) \cdot \frac{\delta}{\sqrt{2\pi y^3}} \exp\left(-\frac{1}{2}\left(\sqrt{y} - \frac{\delta}{\sqrt{y}}\right)\right)^2 dy \\ &= \int_0^{\infty} \frac{\delta}{\sqrt{2\pi z^3}} \exp\left(-\frac{1}{2}\left(\sqrt{z} - \frac{\sqrt{1-2\phi}\delta}{\sqrt{z}}\right)^2 - \frac{1}{2}\sqrt{1-2\phi}\delta + \delta\right) dz \\ &= \exp\left(\delta - \delta\sqrt{1-2\phi}\right).\end{aligned}$$

■

Now we are ready to simplify Terms (A) to (C).

Term (A):

$$\begin{aligned}&\mathbb{E}_t\left[\exp\left(\nu_1\sqrt{h_t}z_{1,t+1} + \nu_2\alpha\left(z_{2,t+1} - \gamma\sqrt{h_t}\right)^2\right)\right] \\ &\quad = \exp\left(-\frac{1}{2}\log\left(1 - 2\nu_2\alpha\left(1-\rho^2\right)\right) - \frac{1}{2}\log\left(1-2m_1\right) + \left(m_3 + \frac{m_2^2}{2\left(1-2m_1\right)}\right)h_t\right),\end{aligned} \tag{B-2}$$

with

$$m_1 = \frac{\nu_2\alpha\rho^2}{1 - 2\nu_2\alpha\left(1-\rho^2\right)}, \tag{B-3}$$

$$m_2 = \nu_1 - \frac{2\rho\gamma\nu_2\alpha}{1 - 2\nu_2\alpha\left(1-\rho^2\right)}, \tag{B-4}$$

$$m_3 = \frac{\gamma^2\nu_2\alpha}{1 - 2\nu_2\alpha\left(1-\rho^2\right)}. \tag{B-5}$$

Term (B) and Term (C):

$$\mathbb{E}_t\left[\exp\left(\nu_1\eta_1 y_{1,t+1}\right)\right] = \exp\left(s_t - s_t\sqrt{1-2\nu_1\eta_1}\right), \tag{B-6}$$

$$\mathbb{E}_t\left[\exp\left(\nu_3 c y_{2,t+1}\right)\right] = \exp\left(s_t - s_t\sqrt{1-2\nu_3 c}\right). \tag{B-7}$$

Then, (A) $\times$ (B) $\times$ (C) yields

$$\exp\left(\begin{array}{c}\left(m_3 + \frac{m_2^2}{2(1-2m_1)}\right)h_t \\ +\left(2-\sqrt{1-2\nu_1\eta_1}-\sqrt{1-2\nu_3 c}\right)s_t \\ -\frac{1}{2}\log\left(1-2\nu_2\alpha\left(1-\rho^2\right)\right)-\frac{1}{2}\log\left(1-2m_1\right)\end{array}\right). \tag{B-8}$$

Now the one-step-ahead MGF can be written as

$$\mathbb{E}_t\left[\exp\left(\nu_1 R_{t+1}+\nu_2 h_{t+1}+\nu_3 s_{t+1}\right)\right] = \exp\left(A_1(\nu_1,\nu_2,\nu_3)h_t + A_2(\nu_1,\nu_2,\nu_3)s_t + B(\nu_1,\nu_2,\nu_3)\right), \tag{B-9}$$

where

$$\begin{aligned}
A_1(\nu_1,\nu_2,\nu_3) &= \nu_1\left(\lambda_z - \frac{1}{2}\right) + \nu_2\beta + m_3 + \frac{m_2^2}{2\left(1-2m_1\right)}, \\
A_2(\nu_1,\nu_2,\nu_3) &= \nu_1\left(\lambda_y - \xi\right) + \nu_3 b + 2 - \sqrt{1-2\nu_1\eta_1} - \sqrt{1-2\nu_3 c}, \\
B(\nu_1,\nu_2,\nu_3) &= \nu_1 r + \nu_2\omega + \nu_3 w - \frac{1}{2}\log\left(1-2\nu_2\alpha\left(1-\rho^2\right)\right) - \frac{1}{2}\log\left(1-2m_1\right)
\end{aligned}$$

are obtained by ν_1, ν_2, ν_3, and parameters of the DCS model.

Next, we derive the multi-period moment generating function, $\Psi(\cdot)$. Let M denote day-to-maturity, the multi-period MGF keeps an exponentially affine structure,

$$\Psi_{t,t+M}(u) \equiv \mathbb{E}_t\left[\exp\left(u\sum_{j=1}^{M} R_{t+j}\right)\right] = \exp\left(C_1(u,M)h_t + C_2(u,M)s_t + D(u,M)\right).$$

By applying the law of conditional expectation iteration, we have

$$\begin{aligned}
\Psi_{t,t+M+1}(u) &\equiv \mathbb{E}_t\left[\exp\left(u\sum_{j=1}^{M+1}R_{t+j}\right)\right] = \mathbb{E}_t\left[\mathbb{E}_{t+1}\left[\exp\left(u\sum_{j=1}^{M+1}R_{t+j}\right)\right]\right] \\
&= \mathbb{E}_t\left[\exp\left(uR_{t+1}\right)\cdot\mathbb{E}_{t+1}\left[\exp\left(u\sum_{j=2}^{M+1}R_{t+j}\right)\right]\right] \\
&= \mathbb{E}_t\left[\exp\left(uR_{t+1}\right)\cdot\mathbb{E}_{t+1}\left[\exp\left(u\sum_{k=1}^{M}R_{t+1+k}\right)\right]\right] \\
&= \mathbb{E}_t\left[uR_{t+1}+C_1(u,M)h_{t+1}+C_2(u,M)s_{t+1}+D(u,M)\right] \\
&= \exp\begin{pmatrix} A_1(u,C_1(u,M),C_2(u,M))h_t \\ +A_2(u,C_1(u,M),C_2(u,M))s_t \\ +B(u,C_1(u,M),C_2(u,M))+D(u,M)\end{pmatrix}.
\end{aligned} \tag{B-10}$$

The recursive rule can be written as

$$\begin{aligned}
C_1(u,M+1) &= A_1(u,C_1(u,M),C_2(u,M)), \\
C_2(u,M+1) &= A_2(u,C_1(u,M),C_2(u,M)), \\
D(u,M+1) &= B(u,C_1(u,M),C_2(u,M))+D(u,M),
\end{aligned} \tag{B-11}$$

where

$$\begin{aligned}
C_1(u,1) &= A_1(u,0,0), \\
C_2(u,1) &= A_2(u,0,0), \\
D(u,1) &= B(u,0,0).
\end{aligned} \tag{B-12}$$

Appendix C Risk Neutralization

The DCS model has four random shocks, $z_{1,t+1}$, $z_{2,t+1}$, $y_{1,t+1}$, and $y_{2,t+1}$. Therefore, we follow the risk-neutralization method of Christoffersen et al. (2010) and apply the following pricing kernel corresponding to the above four random shocks to derive the dynamics under $\mathbb{Q}$ measure:

$$Z_{t+1} = \frac{\exp\left(\nu_{1,t}z_{1,t+1}+\nu_{2,t}z_{2,t+1}+\nu_{3,t}y_{1,t+1}+\nu_{4,t}y_{2,t+1}\right)}{\mathbb{E}_t\left[\exp\left(\nu_{1,t}z_{1,t+1}+\nu_{2,t}z_{2,t+1}+\nu_{3,t}y_{1,t+1}+\nu_{4,t}y_{2,t+1}\right)\right]}. \tag{C-1}$$

We consider the dependence of $z_{1,t+1}$ and $z_{2,t+1}$, and thus

$$Z_{t+1} = \frac{\exp\left(\nu_{1,t}z_{1,t+1}+\nu_{2,t}z_{2,t+1}+\nu_{3,t}y_{1,t+1}+\nu_{4,t}y_{2,t+1}\right)}{\exp\left(\frac{1}{2}\nu_{1,t}^2+\rho\nu_{1,t}\nu_{2,t}+\frac{1}{2}\nu_{2,t}^2+s_t-s_t\sqrt{1-2\nu_{3,t}}+s_t-s_t\sqrt{1-2\nu_{4,t}}\right)}. \tag{C-2}$$

The no-arbitrage condition, namely that the expectation of returns under $\mathbb{Q}$ measure equals to the risk-free return r, yields

$$\mathbb{E}_t^{\mathbb{Q}}\left[\exp\left(R_{t+1}\right)\right] = \exp(r). \tag{C-3}$$

The pricing kernel Z_{t+1} builds the relationship between $\mathbb{P}$ measure and $\mathbb{Q}$ measure,

$$\mathbb{E}_t^{\mathbb{Q}}\left[\exp\left(R_{t+1}\right)\right] = \mathbb{E}_t\left[Z_{t+1}\exp\left(R_{t+1}\right)\right], \tag{C-4}$$

and thus we have

$$\mathbb{E}_t\left[Z_{t+1}\exp\left(R_{t+1}\right)\right] = \exp(r), \tag{C-5}$$

that is,

$$\mathbb{E}_t\left[\exp\left(\begin{array}{c}\nu_{1,t}z_{1,t+1}+\nu_{2,t}z_{2,t+1}+\nu_{3,t}y_{1,t+1}+\nu_{4,t}y_{2,t+1}\\ -\frac{1}{2}\nu_{1,t}^2-\rho\nu_{1,t}\nu_{2,t}-\frac{1}{2}\nu_{2,t}^2-s_t+s_t\sqrt{1-2\nu_{3,t}}-s_t+s_t\sqrt{1-2\nu_{4,t}}\\ +r+\left(\lambda_z-\frac{1}{2}\right)h_t+\left(\lambda_y-\xi\right)s_t+\sqrt{h_t}z_{1,t+1}+\eta_1 y_{1,t+1}\end{array}\right)\right]=\exp(r). \tag{C-6}$$

Therefore, the equivalent condition of the no-arbitrage condition is

$$\nu_{1,t}\sqrt{h_t}+\rho\nu_{2,t}\sqrt{h_t}+\lambda_z h_t - s_t\sqrt{1-2\left(\nu_{3,t}+\eta_1\right)}+s_t\sqrt{1-2\nu_{3,t}}+\left(\lambda_y-\xi\right)s_t=0. \tag{C-7}$$

Similarly, the risk-neutral MGF for random shocks is given by

$$\begin{aligned}&\mathbb{E}_t^{\mathbb{Q}}\left[\exp\left(u_1 z_{1,t+1}+u_2 z_{2,t+1}+u_3 y_{1,t+1}+u_4 y_{2,t+1}\right)\right]\\ &=\exp\left(\begin{array}{c}\frac{1}{2}u_1^2+\left(u_1+\rho u_2\right)\nu_{1,t}+\frac{1}{2}u_2^2+\left(u_2+\rho u_1\right)\nu_{2,t}+\rho u_1 u_2\\ -s_t\sqrt{1-2\left(\nu_{3,t}+u_3\right)}+s_t\sqrt{1-2\nu_{3,t}}-s_t\sqrt{1-2\left(\nu_{4,t}+u_4\right)}+s_t\sqrt{1-2\nu_{4,t}}\end{array}\right).\end{aligned} \tag{C-8}$$

This implies the mapping relationship of random shocks under $\mathbb{P}$ measure and those under $\mathbb{Q}$ measure:

$$\begin{aligned}z_{1,t+1}^* &= z_{1,t+1}-\left(\nu_{1,t}+\rho\nu_{2,t}\right),\\ z_{2,t+1}^* &= z_{2,t+1}-\left(\rho\nu_{1,t}+\nu_{2,t}\right),\\ y_{1,t+1}^* &= \left(1-2\nu_{3,t}\right)y_{1,t+1},\\ y_{2,t+1}^* &= \left(1-2\nu_{4,t}\right)y_{2,t+1},\end{aligned} \tag{C-9}$$

and $\nu_{3,t} = \nu_{4,t}$.

Consequently, combining Equation (C-7), we can obtain the DCS model under $\mathbb{Q}$ measure:

$$R_{t+1} = r - \frac{1}{2}h_t - \xi^* s_t^* + \sqrt{h_t} z_{1,t+1}^* + \eta_1^* y_{1,t+1}^*, \tag{C-10}$$

where

$$\xi^* = 1 - \sqrt{1 - 2\eta_1^*}, \quad s_t^* = s_t\sqrt{1 - 2\nu_{3,t}}, \quad \eta_1^* = \frac{\eta_1}{1 - 2\nu_{3,t}}.$$

Based on the mapping relationship (C-9), the dynamic equation of h_t under $\mathbb{Q}$ measure can be written as

$$h_{t+1} = \omega + \beta h_t + \alpha\left(z_{2,t+1}^* - \gamma_t^*\sqrt{h_t}\right)^2, \tag{C-11}$$

where $\gamma_t^* = \gamma - \frac{\rho\nu_{1,t}+\nu_{2,t}}{\sqrt{h_t}}$. In order to keep the model affine, we set $\nu_{1,t}+\rho\nu_{2,t} = \chi_1$ and $\rho\nu_{1,t}+\nu_{2,t} = \chi_2\sqrt{h_t}$, then

$$\gamma_t^* = \gamma^* = \gamma - \chi_2, \tag{C-12}$$

where χs are parameters of risk premium to be estimated. Therefore, the measurement equation of $\widetilde{\mathrm{RV}}_{t+1}$ under $\mathbb{Q}$ measure is

$$\widetilde{\mathrm{RV}}_{t+1} = h_t^* + \sigma\left[\left(z_{2,t+1}^* - \gamma^*\sqrt{h_t}\right)^2 - \left(1 + \gamma^2 h_t^*\right)\right], \tag{C-13}$$

where

$$h_t^* = h_t + \sigma\left(\gamma^{*2} - \gamma^2\right)h_t. \tag{C-14}$$

Then, the dynamic equation of the inverse Gaussian shock variance component is equivalent to

$$s_{t+1}^* = w^* + bs_t^* + c^* y_{2,t+1}^*, \tag{C-15}$$

where

$$w^* = \sqrt{1 - 2\nu_{3,t}}w, \quad c^* = \sqrt{1 - 2\nu_{3,t}}c. \tag{C-16}$$

Denote $d^* = \frac{d}{d - d\sqrt{1-2\nu_{3,t}} + \sqrt{1-2\nu_{3,t}}}$, $\widetilde{RS}_{t+1}^* = \frac{\sqrt{1-2\nu_{3,t}}d^*}{d}\widetilde{RS}_{t+1}$, the measurement equation of the realized measure of IG component is

$$\widetilde{RS}_{t+1}^* = s_t^* + d^*\left(y_{2,t+1}^* - s_t^*\right). \tag{C-17}$$